

ARTICLE INFO

Article ID: 04-16-01-0003 © 2023 SAE International doi:10.4271/04-16-01-0003

Closed-Loop Predictive Control of a Multi-mode Engine Including Homogeneous Charge Compression Ignition, Partially Premixed Charge Compression Ignition, and Reactivity Controlled Compression Ignition Modes

Sadaf Batool, 1 Jeffrey Naber, 1 and Mahdi Shahbakhti 2

¹Michigan Technological University, USA ²University of Alberta, Canada

Abstract

High thermal efficiency and low engine-out emissions including nitrogen oxides (NOx) and particulate matter (PM) make low-temperature combustion (LTC) favorable for use in engine technologies. Homogeneous charge compression ignition (HCCI), partially premixed charge compression ignition (PPCI), and reactivity controlled compression ignition (RCCI) are among the common LTC modes. These three LTC modes can be achieved on the same dual-fuel engine platform; thus, an engine controller can choose the best LTC mode for each target engine load and speed. To this end, a multi-mode engine controller is needed to adjust the engine control variables for each LTC mode.

This article presents a model-based control development of a 2.0-liter multi-mode LTC engine for cycle-to-cycle combustion control. The engine is equipped with port fuel injectors (PFI) and direct injectors (DI). All combustion modes are achieved with dual fuels (iso-octane and *n*-heptane) under naturally aspirated conditions. Using experimental data, control-oriented models (COMs) are developed for HCCI, PPCI, and RCCI combustion modes on a cycle-to-cycle basis. The COMs for HCCI, PPCI, and RCCI modes can predict the combustion phasing (CA50, the crank angle by which 50% of the fuel mass is burned) with average errors of 1.3 crank angle degrees (CAD), 1.5 CAD, and 1 CAD, respectively. The average errors in predicting the indicated mean effective pressure (IMEP) for HCCI, PPCI, and RCCI modes are 18 kPa, 34 kPa, and 43 kPa, respectively. Multi-input and multi-output (MIMO) adaptive model predictive controllers (MPCs) with linear parameter varying (LPV) models are designed for the LTC modes. CA50 and IMEP are controlled by adjusting the premixed ratio (PR) of the fuels, start of injection (SOI) timing, and fuel quantity (FQ). The results show that the designed MPCs are able to track both CA50 and IMEP in all combustion modes, with average tracking errors of less than 1 CAD and 5.2 kPa, respectively.

History

Received: 05 Oct 2021 Revised: 14 Jan 2022 Accepted: 23 Aug 2022 e-Available: 20 Oct 2022

Citation

Batool, S., Naber, J., and Shahbakhti, M., "Closed-Loop Predictive Control of a Multi-mode Engine Including Homogeneous Charge Compression Ignition, Partially Premixed Charge Compression Ignition, and Reactivity Controlled Compression Ignition Modes," SAE Int. J. Fuels Lubr. 16(1):2023, doi:10.4271/04-16-01-0003.

ISSN: 1946-3952 e-ISSN: 1946-3960

This article is part of a Special Issue on Fuels and Combustion Control Strategies for Low-Temperature Combustion Engines.









1

Introduction

dvancements in compression ignition (CI) engine technology have been made to improve efficiency and lowering engine-out emissions. One of the major focuses in improving CI engine technology is toward the development of advanced combustion modes including lowtemperature combustion (LTC) technologies. Light-duty vehicles (LDVs) account for 52% of fuel consumption in the transportation sector [1]. A recent report by the United States (U.S.) Energy Information Administration states that new LDVs running solely on internal combustion engine (ICE) will contribute to 81% of the market share of new vehicles by 2050 [1]. This number goes up to 85% when hybrid electric and plug-in hybrid electric vehicles are taken into account as they also use an ICE [1]. Therefore, it is essential to optimize the advanced ICE combustion regimes including LTC modes to improve the fuel economy of LDVs and to meet the stringent emission legislations. However, the application of each LTC mode is limited due to the narrow optimal load operating range. To this end, developing a multi-mode engine is an appropriate option to take the advantages of LTC modes while providing full speed and load operation. This requires the development of control-oriented models (COMs) and optimal control methods for a multi-mode LTC engine.

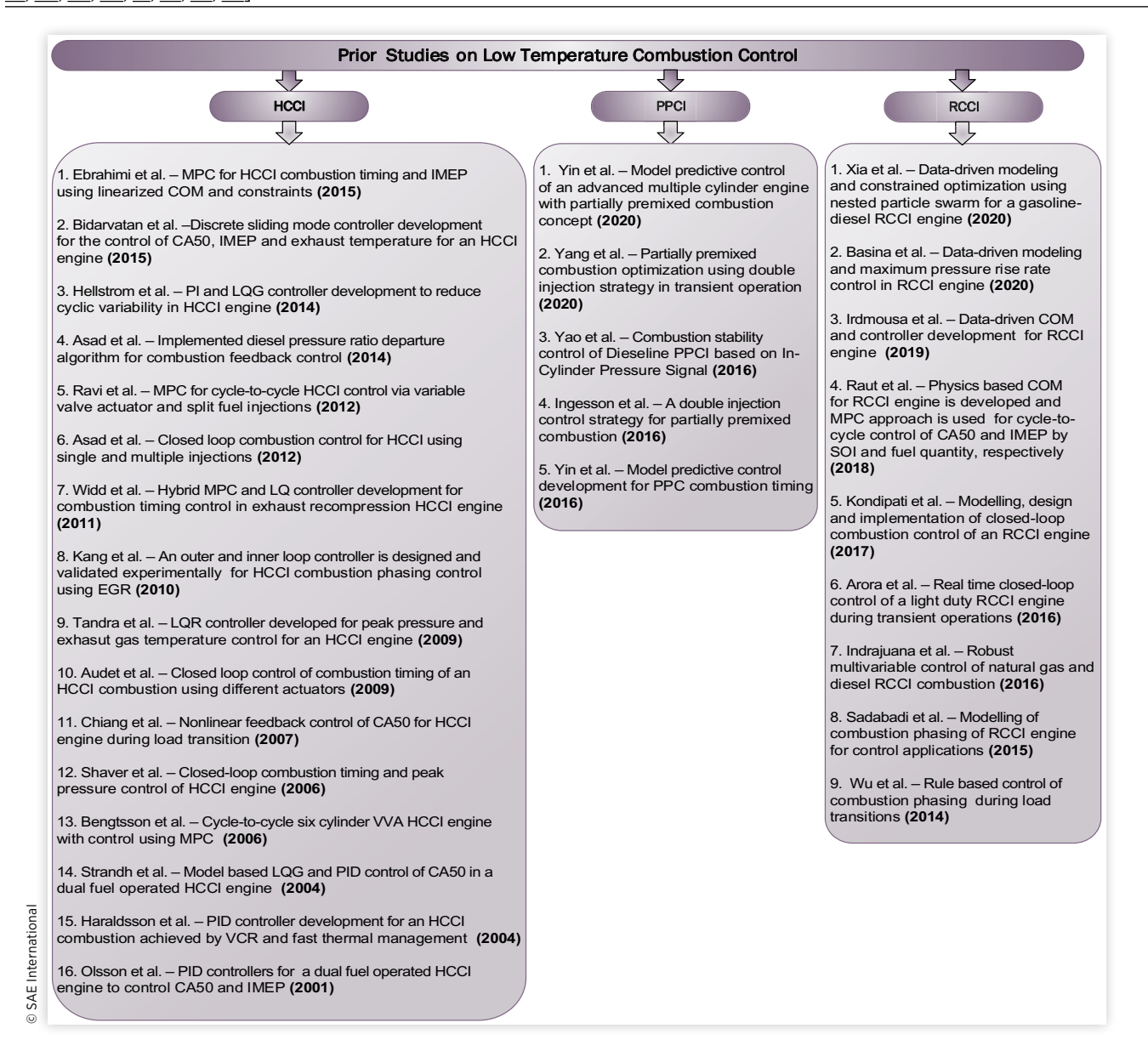
LTC modes generally involve lean premixed mixtures which reduce the local fuel-rich zones. Therefore, too-high peak in-cylinder gas temperatures are avoided that help in restricting nitrogen oxides (NOx) formation. The LTC processes can offer thermal efficiency comparable to conventional diesel combustion engines [2, 3] and produce NOx, and particulate matter (PM) emissions substantially less than conventional CI engines [4, 5]. LTC includes, but is not limited to, homogeneous charge compression ignition (HCCI), partially premixed charge compression ignition (PPCI), and reactivity controlled compression ignition (RCCI) combustion modes [6]. LTC modes can be achieved by using a combination of several strategies such as preheating of the inducted air [7], 8], fast thermal management [9], variable valve actuation [10, 11], variable compression ratio [9, 12, 13], exhaust recompression [11], exhaust gas recirculation (EGR) [7, 8, 14, 15], utilizing dual fuels [2, 15, 16, 17, 18], multiple fuel injections [19, 20], adjusting fuel injection timing [14, 21, 22], and direct dual-fuel stratification [16].

Control of the combustion process in the LTC modes is important to avoid partial burns, misfires, and unsafe high pressure rise rates and knocking [23]. Different LTC modes are achieved using different strategies. For instance, the HCCI mode is more sensitive to the thermodynamic state of the premixed charge (temperature and pressure of the air-fuel mixture) [3, 24]. The mixture in HCCI autoignites in the absence of any external trigger such as a spark in a sparkignition (SI) engine or fuel injection timing in a direct injection (DI) engine [3, 25]. That is why an HCCI combustion event can result in a very rapid rate of heat release causing very high pressure rise rates [25]. This limits the maximum achievable load in an HCCI mode [26]. Therefore, control of

the HCCI process is important for a safe engine operation to avoid too-high pressure rise rates and restrict peak in-cylinder gas pressure. PPCI mode is achieved by injecting the fuel during an early compression stroke. Simultaneous reduction of NOx and soot can be achieved by adding high EGR rates in excess of 70% in a low compression ratio diesel engine running in PPCI mode [27]. However, it is difficult to obtain high EGR rates in excess of 70% from the engine air handling perspective [25]. NOx and smoke can be simultaneously reduced by delaying the heat release to the point where the fuel and air are sufficiently mixed. A study conducted on ethanol PPCI combustion at Lund University achieved low emissions with 40-47% EGR. However, pilot injection timing and pilot-to-main fuel injection ratio were adjusted to limit the pressure rise rates below 10 bar/crank angle degrees (CAD) [4]. Although, PPCI mode offers low engine-out emissions, the control of combustion timing and heat release rate is challenging. The maximum work output reduces by retarding the heat release, therefore resulting in a trade-off between thermal efficiency and combustion noise [16].

RCCI mode is realized by using dual fuels of different reactivity levels. This combustion mode offers high thermal efficiency along with low NOx emissions [21, 28, 29]. The ratio of high- to low-reactivity fuel provides control over the heat release rate, which results in controlled combustion noise levels [16]. Splitter et al. explored the effect of injections on a low-load RCCI operation and found that double injections reduced carbon monoxide (CO) and hydrocarbon (HC) emissions to 40% [30]. Wu et al. proposed that combustion phasing can be controlled by changing the port fuel injection (PFI) fuel ratio during load transients [31]. To ensure stable and controlled combustion, it is imperative to control the combustion phasing and load in the LTC modes. Various studies have been conducted on the modeling and control development of the LTC modes. An overview of prior control studies carried out on LTC modes is presented in Figure 1. These studies are grouped into HCCI, PPCI, and RCCI combustion modes. Here, a brief review of each group is provided. Combustion phasing and indicated mean effective pressure (IMEP) are the two important control parameters. Combustion in an LTC engine is sensitive to the change in the thermodynamic states at the intake valve closing (IVC), such as intake air temperature and residual gas fraction. Uncontrolled combustion may lead to knocking due to advanced combustion phasing or even a misfire in case of a too retarded combustion [28]. CA50 (the crank angle by which 50% of the fuel mass is burned) is an important parameter that directly influences the IMEP, maximum pressure rise rate (MPRR), exhaust gas temperature, and CO and unburned HC emissions [32]. Furthermore, partial or incomplete combustion results in a lower IMEP. This usually causes the next engine cycle to produce a higher IMEP because of the unburned fuel from the previous engine cycle. This leads to an increased coefficient of variation of IMEP (COV_{IMEP}) which affects the noise, vibration, and harshness (NVH) performance of the vehicle. Therefore, it is important to simultaneously control CA50 and IMEP for optimum and safe engine operation.

FIGURE 1 Prior studies on the control of LTC modes [6, 9, 14, 15, 19, 21, 28, 31, 33, 34, 35, 36, 37, 38, 39, 40, 41, 42, 43, 44, 45, 46, 47, 48, 49, 50, 51, 52, 53, 54].



LTC modes can be modeled by using computational fluid dynamics (CFD) and detailed kinetic reaction mechanisms to analyze the combustion dynamics and prediction. Wu et al. proposed that combustion phasing can be controlled by changing the PFI fuel ratio during load transients in the RCCI mode [31]. A multi-dimensional CFD model coupled with a kinetics-based combustion model was used to control combustion phasing during load transition. The computation time of this numerical-based study was around 15 h for each case, using three central processing units. Eichmeier et al. developed a zero-dimensional phenomenological RCCI combustion model, and the results were compared with experimental data and a three-dimensional (3D) CFD model. The

zero-dimensional model was based on a reduced-order mechanism, and each zone was considered a constant volume reactor. Computational time was sufficiently reduced by running the reaction kinetics parallel and using the iteration scheme. The study mentioned that both the 3D CFD and zero-dimensional models were highly dependent on the initial conditions at IVC. The zero-dimensional model requires an accurate knowledge of the initial conditions The prediction accuracy of the developed zero-dimensional model is dependent on the accurate knowledge of the initial conditions [55]. Numerical studies require extensive computational resources and run-time, which make them less appropriate for real-time control applications. Therefore, the present study introduces

a computationally efficient physics-based control-oriented modeling (COM) approach for real-time control of LTC modes on a cycle-to-cycle basis.

A wide range of studies have been conducted on COM and controller development for the HCCI mode. The COM of the HCCI combustion includes prediction of ignition timing [24, 56], combustion phasing [10, 57, 58, 59, 60], load [56, 60, 61], combustion efficiency [60], exhaust gas temperature, and engine-out emissions [61]. Olsson et al. developed proportional integral derivative (PID) controllers for a dual-fuel HCCI operation to control heating, combustion timing, and IMEP [33]. Haraldsson et al. also implemented PID controllers using variable compression ratio and fast thermal heating as manipulated variables for combustion timing control and adjusted fuel quantity (FQ) for load control [9]. Manual PID and linear quadratic Gaussian (LQG) model-based controllers were developed for an HCCI engine using dual fuels. Strandh et al. compared the performance of PID and LQG controllers along with the performance comparison of the feedback signals from pressure and ion current sensors. The study concluded that both controllers worked well for combustion timing control [34].

Bengtsson et al. used system identification to model an HCCI engine with variable valve actuation. The study incorporated a model predictive control (MPC) framework for multi-input and multi-output (MIMO) control of an HCCI engine with constraints on control variables and pressure rise rate $(dP/d\theta)$ [35]. Widd et al. compared the performance of hybrid MPC and switched the LQ controller for the combustion timing control of the exhaust recompression HCCI. Due to optimal control provided by the MPC over the prediction horizon, the MPC response showed no overshoot while the LQ controller response resulted in a large overshoot [36]. Ravi et al. demonstrated an LQR controller that is developed based on a physics-based two-state COM for an exhaust recompression HCCI combustion mode in a gasoline engine [62]. Shaver et al. controlled peak pressure and combustion timing using an H_2 optimal controller for a residual-affected HCCI engine. The inducted gas composition and effective compression ratio were used as control knobs [37]. A study conducted by Kang et al. showed that the mass fraction of burned gases in the intake and exhaust ports can also be used to control combustion phasing indirectly in the HCCI mode [38]. Ravi et al. used an MPC framework to control the combustion phasing (CA50) and net mean effective pressure (NMEP) for an HCCI engine. This study used a variable valve actuation system and split fuel injection strategy to control HCCI. In addition, constraints on the injection timing, cylinder volume at intake and exhaust valve closure and maximum allowable rate of change of valve timings, and air-to-fuel ratio (AFR) were implemented. The AFR was constrained to avoid too lean or too rich of a mixture. The controller response for tracking the NMEP became slower with the application of constraints on the AFR [19]. Ebrahimi et al. implemented MPC to control combustion phasing and load by adjusting valve timing and fueling rate [39]. In order to avoid misfire or ringing, constraints were applied on the combustion phasing and load. Bidarvatan et al. developed a

sliding mode controller to control combustion phasing, load, and exhaust gas temperature for a stable HCCI engine operation [40]. This robust discrete suboptimal sliding mode controller performed well in the presence of disturbances and showed no steady-state errors.

There are several studies conducted on the modeling and control of PPCI engines. Hall et al. developed a COM for start of combustion (SOC) prediction for a PCCI engine [63]. Tunestal et al. used system identification to model PPCI combustion [64]. Yao et al. developed a closed-loop feedback controller for combustion stability and combustion noise level control for a PPCI engine. Injection timings and EGR (%) were used to control the MPRR and COV_{IMEP} . The MPRR and COV_{IMEP} were chosen as representatives of combustion noise level and combustion stability, respectively [14]. Ingesson et al. implemented an MPC to limit MPRR while controlling CA50 by adjusting the pilot ratio and timing of the main injection for PPCI operation. The fuel being used was composed of 80% gasoline and 20% *n*-heptane by volume. A split injection (an early pilot injection followed by the main injection) strategy was used to reduce ignition delay which resulted in a low MPRR [41]. Yin et al. developed a PPCI combustion control system for a heavy-duty 13-liter diesel engine using a fuel blend (80% gasoline and 20% n-heptane). A triple-injection strategy was employed along with 45-50% EGR. The study incorporated an MPC for a transient load range of 4-15 bar at 1200 revolutions per minute (RPM). The controller results showed a trade-off between faster response and overshoot [15]. Yang et al. employed a double-injection strategy for PPCI operation. An MPC framework was implemented for CA50 and IMEP control including constraints on MPRR, soot, and NOx. The study included a 5 bar to 8 bar IMEP range of transient PPCI operation at a constant engine speed of 1200 RPM [42].

Researchers have also explored control of RCCI engine operation using various feedback controllers including proportional integral (PI), linear quadratic regulator (LQI), and MPC. There are various parameters that can be used to control combustion phasing in the RCCI mode. These parameters include start of injection (SOI), dual-fuel premixed ratio (PR), split injections, valve timings, etc. Kondipati et al. designed a PI controller to control CA50 for an RCCI engine using either PR or SOI as control inputs [43]. Arora et al. carried out an experimental study on mode switching for RCCI-SI-RCCI [6]. A PI controller along with feedforward control was implemented for cycle-to-cycle control of CA50 during transient operation [6]. An observer-based LQI controller was developed to control CA50 using PR as the control input. Observer performance under transient RCCI operation was also examined [44]. The results showed no steady-state tracking errors and good disturbance rejection performance. Indrajuana et al. investigated RCCI combustion using natural gas and diesel [28]. RCCI operation was controlled on a cycle-to-cycle basis by using diesel injection timing, diesel FQ, and natural gas FQ. A robust MIMO feedback controller was developed for engine load, ignition delay, and blend ratio control to achieve low NOx emissions

[28]. Raut et al. implemented multiple model predictive controllers (MPCs) to control engine load and CA50 during the transient operation of an RCCI engine [21]. SOI was used as control input for adjusting CA50 while FQ was used to control the engine load. Moreover, PR was used as a scheduling variable for switching between multiple MPCs to increase the operating range of the RCCI engine [21]. Irdmousa et al. developed a data-driven COM for an RCCI engine using FQ as the scheduling variable. This study incorporated a linear parameter varying (LPV) model along with MPC for CA50 control. The controller developed on the datadriven model showed a similar response as compared to physics-based MPC [51]. Batool et al. developed data-driven classification models for COV_{IMEP} for HCCI and RCCI modes [65]. CA50 and IMEP were regulated by designing nonlinear MPC frameworks for HCCI and RCCI modes while constraining COV_{IMEP} below 3% [65].

Despite the benefits of high efficiency and ultralow NOx and soot emissions, LTC modes can suffer from a limited load operation. To address this shortcoming, several studies have been conducted on mode switching between LTC and conventional SI and CI modes. Widd et al. studied SI to HCCI mode switching. A model-based controller was designed, and its results showed better performance as compared to PI controllers [66]. Roelle et al. developed a multi-mode combustion model for SI to HCCI transition [67]. Gorzelic et al. implemented a model-based feedback control for SI-HCCI mode transition [3]. An online parameter adapting algorithm was appended to the model-based control platform to reduce the errors while improving robustness and addressing the cylinderto-cylinder variability. Nuesch et al. developed a finite-state machine model to capture HCCI-SI mode-switching dynamics and fuel penalties [68]. Besides the significant reduction in NOx emissions and improvement in fuel efficiency in the HCCI mode, the mode switching induces penalties in fuel efficiency while meeting the high torque requests.

This article presents a unified modeling and control platform to adjust combustion phasing and load for three LTC modes on the same engine platform. To the best of the authors' knowledge, this work is the first study undertaken to control three LTC modes with an integrated optimal and predictive control setup. An optimizer selects the best LTC mode and the designed multi-mode MPC combustion controller adjusts the SOI, PR, and FQ to control CA50 and IMEP. The multimode controller focuses on optimal LTC operation in each mode, while mode-switching control is outside the scope of this article. All three modes are achieved on a single engine. The three different LTC modes are achieved using different strategies, and each mode offers different challenges. That is why it is difficult to have a single controller framework for all LTC modes. LPV models are identified to capture the LTC dynamics and then LPV models are incorporated into the MPC framework to provide a wide operating range. The designed controllers are also tested for disturbance rejection properties.

The major contributions in this article include (i) A unified modeling platform is developed to include

physics-based COMs for the three LTC modes to control the combustion phasing and load for a range of PRs. The models are validated for stead-state and transient conditions; (ii) Three MIMO adaptive MPCs are developed for the LTC modes. In order to address the nonlinear behavior of dual-fuel combustion with varying PR and to improve the controller response for a wide range of load operations, LPV models are developed. These LPV models are integrated into the adaptive MPC framework. LPV models are developed for different PRs which capture the nonlinear dynamics of the LTC modes. The LPV models are then used within the adaptive MPC framework to extend the operating range and improve the performance of the controller; (iii) The disturbance rejection performance of the developed MIMO adaptive MPCs is verified.

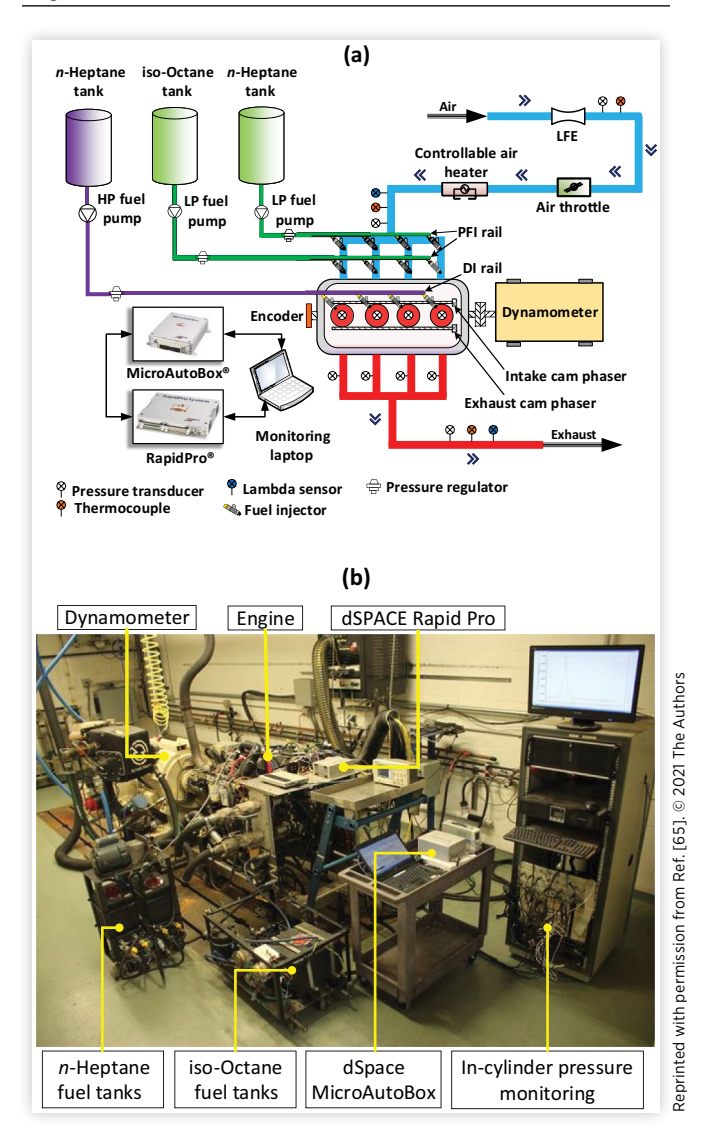
The organization of this article is as follows: Section II explains the experimental setup and the specifications of the engine used to collect the experimental data for LTC modes. This section also includes the operating conditions for each mode. Section III explains the development of COMs for each mode on a cycle-to-cycle basis. The following Section IV focuses on the development of LPV systems and adaptive MPCs. MPCs and Kalman filters are designed for optimum performance in each mode. Section V presents results and discussions for multi-mode engine operation. The disturbance rejection performance of controllers is also assessed. The last section summarizes the major findings from this study and provides recommendations for future studies.

Experimental Setup and Engine Data

A GM Ecotec 2.0L engine is used for conducting the experiments, coupled with an AC dynamometer of 460 hp. The original GDI engine with one DI system is modified to include two PFI systems and use the original DI system, as shown in <u>Figure 2</u>. Engine specifications are given in <u>Table 1</u>. The engine is run at naturally aspirated conditions without EGR. PCB piezoelectric pressure transducers are used to measure in-cylinder gas pressure with a resolution of 1 CAD. A dSPACE MicroAutoBox is used as the engine control unit. For the real-time feedback of combustion parameters, Xilinx Spartan-6 field programmable gate array is used. The intake air is preheated to the desired temperature with the help of an external air heater. Meriam MDT500 airflow measurement system is used to measure the mass flow rate of the intake air. More details about the engine instrumentation can be found in reference [69].

The engine is run in three LTC modes including HCCI, PPCI, and RCCI by adjusting the engine variables and using dual fuels, i.e., *n*-heptane and iso-octane. In HCCI mode, both iso-octane and *n*-heptane are injected into intake ports during the exhaust stroke of the previous cycle via two PFI systems. While *n*-heptane is directly injected during the compression stroke for PPCI and RCCI modes. In PPCI mode, the SOI is

FIGURE 2 Experimental setup of the multi-mode LTC engine.



kept constant at 100 CAD before top dead center (bTDC); while in RCCI mode, the SOI of *n*-heptane is varied. For HCCI, PPCI, and RCCI combustion modes, intake air temperature, total FQ, and the PR of fuels are varied. The PR of the two fuels is calculated using the following equation:

$$PR = \frac{m_{iso}LHV_{iso}}{m_{iso}LHV_{iso} + m_{nhep}LHV_{nhep}}$$
 Eq. (1)

where m_{iso} and $m_{n hep}$ are the mass of injected iso-octane and n-heptane, respectively. LHV_{iso} and $LHV_{n hep}$ are the lower heating values of iso-octane and n-heptane, respectively.

Performance maps for the LTC modes are shown in Figure 3 on the basis of brake specific fuel consumption (BSFC). Based on the comparison with the baseline SI map, HCCI combustion in this engine shows a 9% improvement in BSFC at low loads for a speed range of 800-1600 RPM.

TABLE 1 Engine specifications.

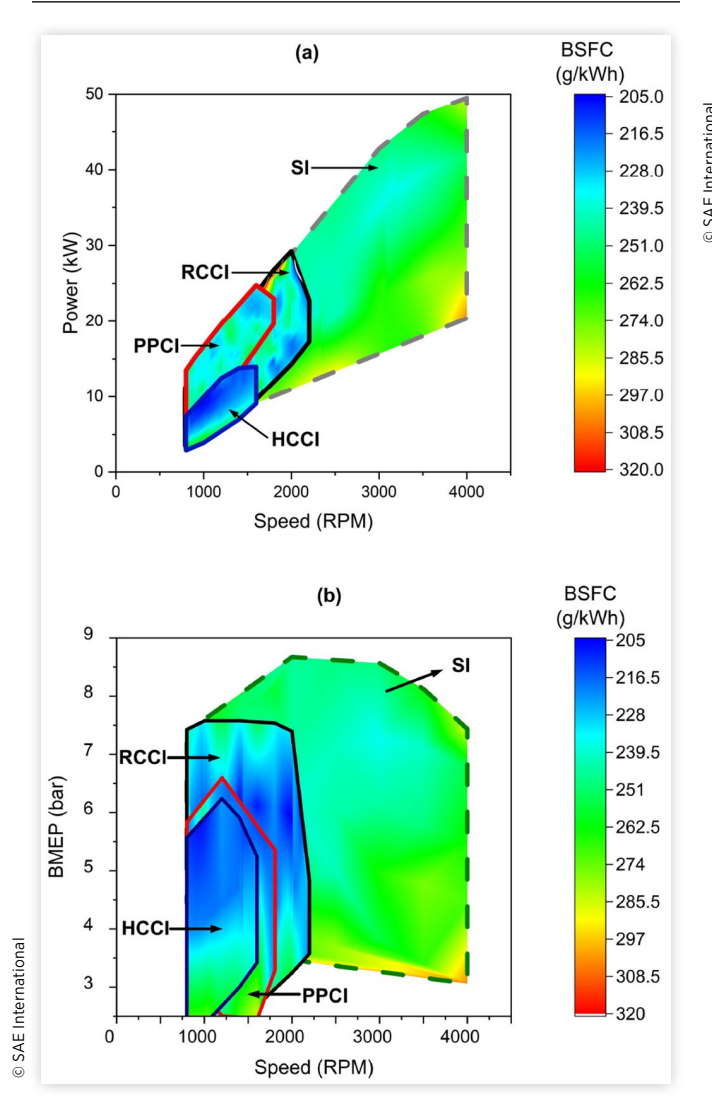
Engine type	GDI, 4 stroke	
No. of cylinders	4	
Cylinder volume	1998 (cc)	
Bore	86 (mm)	
Stroke	86 (mm)	
Compression ratio	9.2:1	
IVO	25.5/-24.5 (CAD bTDC)	
IVC	2/-48 (CAD bBDC)	
EVO	36/-14 (CAD bBDC)	
EVC	22/-28 (CAD bTDC)	
Valve lift	10.3 (mm)	_
Max. engine power	164 kW at 5300 RPM	tiona
Max. engine torque	353 Nm at 2400 RPM	erna
Intake valve diameter	35.17 (mm)	SAE Internationa
Firing order	1-3-4-2	© SA

PPCI mode offers a 5% improvement at 6 bar when compared to the baseline SI engine. RCCI combustion shows up to 14% improvement in BSFC for a load range of 6-8 bar as compared to the baseline SI mode. This article focuses on developing a model-based control platform to allow optimal engine operation in HCCI, PPCI, and RCCI modes based on the requested speed and load conditions to offer the best BSFC.

The operating conditions of the data used in this study are shown in <u>Table 2</u>. The measured uncertainties in the values of CA50 and IMEP calculated from the experimental data are 1 CAD and 7.7 kPa, respectively [69].

In-cylinder gas pressure (solid lines) and the resulting rate of heat release (dotted lines) in the LTC modes are shown in Figure 4 for a sample operating condition for comparison. Combustion in HCCI mode occurs predominantly in two stages because of early injections and the homogeneous air-fuel mixture. First-stage heat release corresponds to the low-temperature reactions while the high-temperature reactions result in the second-stage combustion. High-temperature heat release (HTHR) followed by low-temperature heat release (LTHR) is more abrupt in HCCI mode. Ignition in PPCI mode also occurs in two stages. The LTHR in the heat release rate of HCCI mode seems higher than the one in PPCI mode. However, the magnitude of heat released in HCCI mode during lowtemperature reactions is lower than that of the PPCI mode. The cumulative LTHR in PPCI and HCCI modes are 98 J and 53.4 J, respectively. However, the HTHR in PPCI mode is less rapid resulting in relatively late combustion phasing as compared to HCCI mode. Due to the late injection of n-heptane, RCCI mode does not exhibit abrupt heat release rate. In addition, combustion in RCCI mode happens in a single stage with late combustion phasing compared to HCCI and PPCI modes. That is why SOI proves to be an effective control knob in single-stage heat release in RCCI combustion along with PR.

FIGURE 3 Comparison of the engine tested conditions for SI, HCCI, PPCI, and RCCI modes.



COMs for Combustion Modes

Dynamic models of the LTC modes need to represent the entire engine cycle. The process starts from mode selection based on the requested speed and load followed by the intake valve opening (IVO) to exhaust valve closing (EVC) events, as shown in Figure 5. This study is based on three different LTC modes, which is why the particular mode offering the lowest BSFC is first selected from the engine map as shown in Figure 3. Modes 1, 2, and 3 represent HCCI, PPCI, and RCCI, respectively. Step 1 is the mode selection. Based on the mode number, the particular dynamic model is selected to represent the corresponding engine operation. Step 2 includes the IVO to IVC event. The pressure and temperature of the air-fuel mixture at IVC for all combustion modes are estimated using Equations 2 and 3,

TABLE 2 Range of experimental data used for the COM development of the LTC modes.

	Parameters	нссі	PPCI	RCCI
	IAT (°C)	40:20:100	40:20:100	40:20:80
=	P _{man} (kPa)	96	96	96
International	Engine speed (RPM)	800	800	1000
erna	PR (-)	0-40	0-40	10-40
SAE Int	SOI (CAD bTDC)	450	100	20-60
S S ⊚	Equivalence ratio, ϕ (—)	0.32-0.67	0.3-0.8	0.32-1.00

respectively. To incorporate cycle-to-cycle coupling, the temperature at IVC is calculated by taking the residual gas fraction and the residual gas temperature into account.

$$P_{ivc} = \frac{N^a \phi^b}{T_{...}^c} P_m, \qquad \text{Eq. (2)}$$

$$T_{ivc} = (1 - X_{rg})T_{in} + X_{rg}T_{rg}$$
 Eq. (3)

where N is the engine speed, P_m is the intake manifold pressure, T_m is the intake manifold temperature, ϕ is the fuel-air equivalence ratio, T_{rg} is the residual gas temperature, and X_{rg} is the residual gas fraction. X_{rg} for the first cycle is estimated using Equation 4 [18]:

$$X_{rg} = \sqrt{\frac{1}{C}} \cdot \frac{\pi \sqrt{2}}{360} \cdot \frac{r_c - 1}{r_c} \cdot \frac{OF}{N} \cdot \sqrt{\frac{RT_m \left| P_{exh} - P_m \right|}{P_{exh}}}.$$

$$\left(\frac{P_{exh}}{P_m}\right)^{\frac{k_c + 1}{k_c}} + \frac{1}{C} \cdot \frac{r_c - 1}{r_c} \cdot \phi_{tot} \frac{V_{ivo}}{V_d} \cdot \left(\frac{P_{exh}}{P_m}\right)^{\frac{1}{k_c}}$$
Eq. (4)

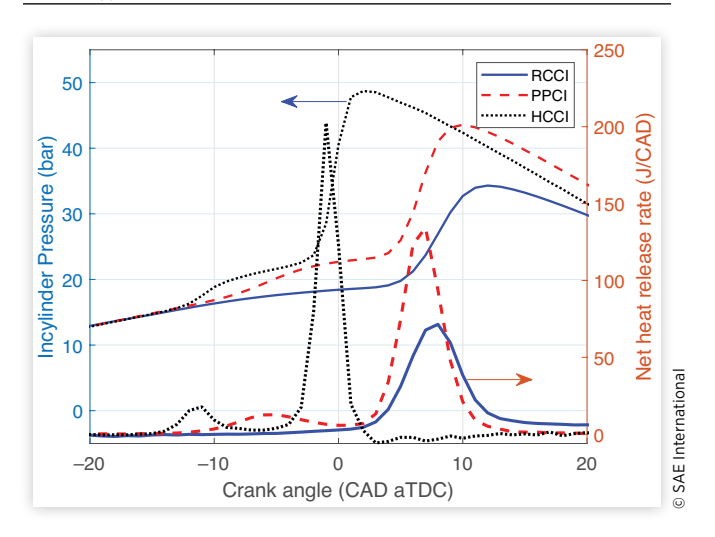
where OF is the overlap factor, r_c is compression ratio, R is gas constant, and V_d is displaced volume. C is given by the following:

$$C = \left[1 + \frac{LHV}{c_{v}T_{m}\frac{m_{t}}{m_{f}} \cdot r_{c}^{k_{c}-1}} \right]^{\frac{1}{k_{c}}}$$
 Eq. (5)

where m_f is the mass of fuel injected and m_t is the sum of the mass of air and mass of fuel.

The air-fuel mixture undergoes autoignition in the LTC modes [70]. The SOC is defined as the crank angle where 10% of fuel mass is burned. SOC is estimated using a modified knock integral model (MKIM) [58]. The MKIM is calibrated for each combustion mode separately such that the integral becomes 1 at SOC. MKIM is integrated from IVC to SOC for the LTC mode using fuel injected via PFI only, using Equation 6. However, the integral of the MKIM is divided into two parts for the LTC modes using both PFI and DI as shown in Equation 7 [21]. The first part in Equation 7 considers the fuel coming from PFI, thus integrating from IVC to SOI, and the second part in Equation 7 incorporates the effect of directly injected fuel, hence integrating from SOI to SOC.

FIGURE 4 Experimental in-cylinder gas pressure and heat release rate in LTC modes (N = 1000 RPM, PR = 20, $T_{man} = 313$ K, $SOI_{RCCI} = 25$ CAD [bTDC], $\Phi = 0.65$).



$$\int_{\theta_{ivc}}^{\theta_{exc}} \frac{\phi_k^A}{B \exp\left(\frac{C\left(P_{ivc,k+1}v_c^k\right)^D}{T_{ivc}V_c^kc^{-1}}\right)N_k} d\theta = 1$$
 Eq. (6)

$$\int_{\theta_{ivc}}^{\theta_{soi}} \frac{d\theta}{B_{1}\phi_{PFI}^{A_{1}} \exp\left(\frac{C_{1}\left(P_{ivc,k+1}v_{c}^{k}\right)^{D_{1}}}{T_{ivc}V_{c}^{k}c^{-1}}\right)N_{k}} + \int_{\theta_{soi}}^{\theta_{soi}} \frac{d\theta}{B_{2}\left(\phi_{PFI}^{A_{2}} + \phi_{DI}^{A_{3}}\right) \exp\left(\frac{C_{2}}{CN_{mix} + E}\right)\left(P_{ivc,k+1}v_{c}^{k}\right)^{D_{2}}}{T_{ivc}V_{c}^{k}c^{-1}}\right)N_{k}} = 1$$
Eq. (7)

$$\phi_{DI} = (1 - PR) \cdot \phi \qquad \text{Eq. (8)}$$

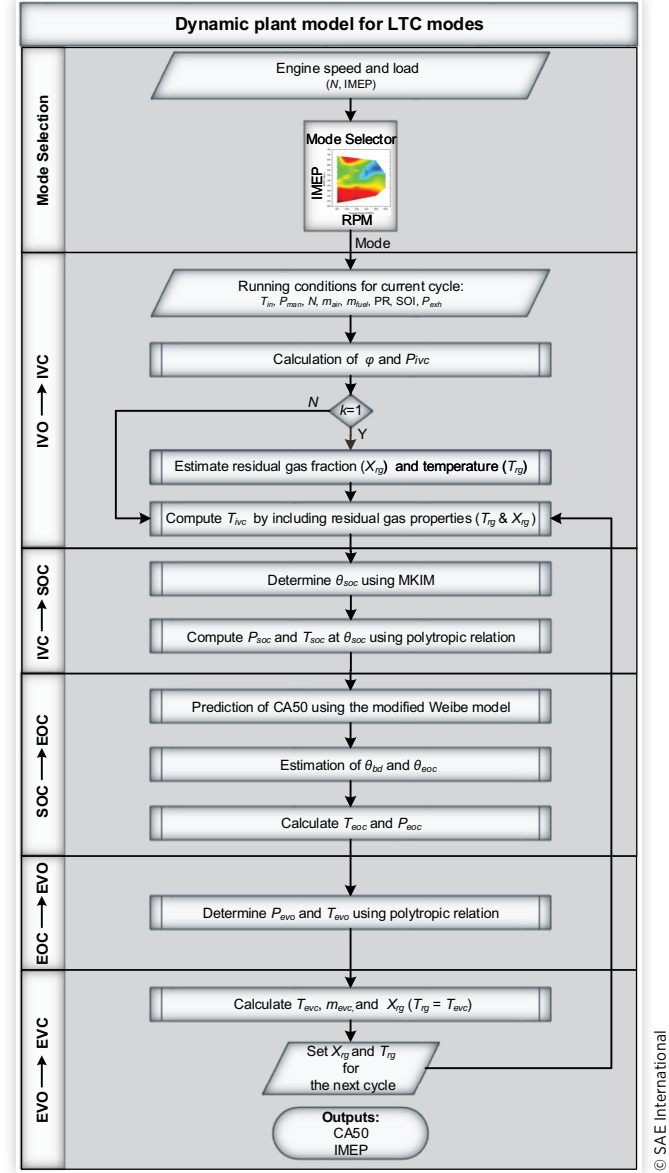
$$\phi_{PFI} = PR \cdot \phi$$
 Eq. (9)

where A, A_1 , A_2 , A_3 , B, B_1 , B_2 , C, C_1 , C_2 , D, D_1 , D_2 , and E are the parameters estimated by calibrating the MKIM for the LTC modes. ϕ , in Equation 6, is the total equivalence ratio of the injected fuels. ϕ_{PFI} and ϕ_{DI} are the equivalence ratios of iso-octane and n-heptane, respectively.

Pressure (P_{soc}) and temperature (T_{soc}) at SOC are calculated using a polytropic relationship, using Equations 10 and 11.

$$P_{soc} = P_{ivc} \left(\frac{V_{ivc}}{V_{soc}} \right)^{k_c}$$
 Eq. (10)

FIGURE 5 Designed multi-mode dynamic model for the LTC engine.



$$T_{soc} = T_{ivc} \left(\frac{V_{ivc}}{V_{soc}} \right)^{k_c - 1}$$
Eq. (11)

where k_c is the polytropic index of compression. V_{ivc} and V_{soc} are the volumes at IVC and SOC, respectively.

The Wiebe function is parameterized for each LTC mode for the estimation of CA50, using Equation 12. CA50 is defined as the crank angle by which 50% of the fuel mass is burned.

$$x_b(\theta) = 1 - \exp\left(-a\left[\frac{\theta - \theta_{soc}}{\theta_d}\right]^n\right)$$
 Eq. (12)

$$\theta_d = CD \left(1 + X_d \right)^x \phi^y$$
 Eq. (13)

$$X_d = EGR + \frac{X_{rg}}{1 - X_{rg}}$$
 Eq. (14)

where a and n are the constants calculated by parameterizing the Wiebe function. θ_d is the burn duration estimated by using Equation 13. X_{rg} is the residual gas fraction. The temperature at the end of combustion (T_{eoc}) is calculated from the temperature rise due to the fuel burned during combustion, using Equation 15.

$$T_{eoc} = T_{soc} + \Delta T$$
 Eq. (15)

$$\Delta T_{comb} = \frac{LHV_f CoC}{(1 + X_{re})(\phi^{-1}AFR_{st} + 1)C_{\nu}}$$
 Eq. (16)

$$P_{eoc} = \frac{P_{soc}V_{eoc}}{V_{eoc}} \frac{T_{eoc}R_{eoc}}{T_{soc}R_{soc}}$$
Eq. (17)

where CoC is the completeness of combustion, AFR_{st} is the stoichiometric AFR. Pressure and temperature at the end of the expansion stroke are calculated using a polytropic relationship, as shown in Equations 18 and 19, respectively.

$$P_{evo} = P_{eoc} \left(\frac{V_{eoc}}{V_{evc}} \right)^{k_e}$$
 Eq. (18)

$$T_{evo} = T_{eoc} \left(\frac{V_{eoc}}{V_{evo}} \right)^{k_e - 1}$$
 Eq. (19)

where k_e is the polytropic index of expansion, while V_{evo} and V_{evc} are the volumes at end of combustion (EOC) and exhaust valve opening (EVO), respectively. The temperature of the in-cylinder charge at the end of EVC is calculated using Equation 20:

$$T_{evc} = T_{evo} \left(\frac{V_{evo}}{V_{evc}} \right)^{k_e - 1}$$
Eq. (20)

where T_{evc} is the temperature at EVC, V_{evo} and V_{evc} in Equation 20 are the volumes at EVO and EVC, respectively. The mass of residual gases (m_{evc}) trapped in the cylinder at EVC is calculated using Equation 21:

$$m_{evc} = \frac{P_{exh}V_{evc}}{R_{evc}T_{evc}}$$
 Eq. (21)

where P_{exh} is the exhaust pressure, V_{evc} , T_{evc} , and R_{evc} are the volume, temperature, and gas constant at EVC, respectively. Residual gas fraction (X_{rg}) at the end of the engine cycle is calculated using Equation 22:

$$X_{rg} = \frac{m_{evc}}{m}$$
 Eq. (22)

IMEP is calculated using Equation 23 [61]. m_t is the sum of the mass of air, fuel, and residual gas fraction of the current cycle:

$$IMEP = m_t \frac{Cv}{V_{dis}} \left(T_{ivc} - T_{soc} + T_{eoc} - T_{evc} \right) \qquad \text{Eq. (23)}$$

Fuel Transport Dynamics

This work includes fuel injection via PFIs; therefore, it is important to consider the port fuel transport dynamics. The fuel injected via PFI undergoes transport dynamics before entering the cylinder. This transport dynamics of the fuel can be explained by the $\tau-X$ model [71]. A portion of the total injected fuel from the PFI vaporizes and enters the cylinder directly while the remaining forms a puddle in the intake port. The fuel in the puddle evaporates slowly and then enters the cylinder. The rate at which the fuel evaporates from the puddle is proportional to the puddle mass (m_p) and inversely proportional to the evaporation time constant (τ) . The amount of fuel entering the cylinder is determined by using Equation 24:

$$\dot{m}_{cyl} = \frac{1}{\tau} m_p + (1 - X) \dot{m}_{fi}$$
 Eq. (24)

where \dot{m}_{cyl} is the mass of fuel entering the cylinder, X is the fraction of the injected fuel which enters the puddle, and \dot{m}_{fi} is the rate of total fuel injected.

The measurement dynamics and transport delay associated with the lambda sensor and exhaust gas transport delay to reach the lambda sensor. The lambda sensor can be modeled as a first-order dynamic system lag and exhaust gas transport as a time delay. The values of T_L and τ_m are determined by using system identification. Equation 25 shows the transfer function for the lambda sensor model in the Laplace domain.

$$G(s) = \frac{K_p e^{-sT_L}}{\tau \quad s+1}$$
 Eq. (25)

To determine the values of τ and X, the fuel is injected via PFI. System identification is used to determine the values of τ and X using Equation 26:

$$\frac{\dot{m}(s)}{\dot{m}_{f_t}(s)} = \frac{(1+\tau(1-X)s)}{1+\tau s} \frac{1}{1+\tau_{m}s} e^{-sT_L}$$
 Eq. (26)

where \dot{m} is the amount of the fuel calculated using lambda sensor measurements. The values of T_L , τ_m , X, and τ are determined to be 0.15 s, 0.43 s, 0.09 s, and 0.06 s, respectively.

Model Validation

The developed dynamic models for HCCI, PPCI, and RCCI combustion modes are parameterized and validated based on steady-state experimental data. Half of the experimental data is used for parameterization while the other half is used for the model validation. HCCI and PPCI model validations for SOC, burn duration (BD), CA50, and IMEP prediction are shown in Figures 6 and 7, respectively.

The developed models are used as virtual plants for the design and testing of the controller. For transient validation of the HCCI model, step changes in PR and FQ are provided simultaneously (Figure 9). The experimental data and model outputs are compared as shown in Figure 9. It can be observed that the model is capable of responding to the step changes in the PR and FQ. Combustion phasing retards with the increase in PR and IMEP increases as FQ increases. The average error in predicting CA50 is 1 CAD while the average error in predicting IMEP is 24 kPa for HCCI. The RCCI model is also validated under different transient conditions. Experimental data and model outputs for RCCI mode are compared for two different cases as shown in Figures 10 and 11. In the first scenario, a step change in the SOI is provided while keeping the FQ constant for the PR of 20. For the second case, the SOI of 50 CAD bTDC and PR of 20 are kept constant and FQ is varied. It can be seen that the model predicts CA50 and IMEP with average errors of less than 2 CAD and 37 kPa, respectively, for both cases.

State-Space Modeling of LTC Modes

The outputs of the nonlinear COM for HCCI and PPCI modes can be represented on a cycle-to-cycle basis as shown in Equations 34 and 35 whereas outputs for RCCI mode can be represented as shown in Equations 36 and 37. The nonlinear models are computationally expensive. Therefore, the developed nonlinear COMs for CA50 and IMEP control on a cycle-to-cycle basis are linearized around the nominal operating conditions for each LTC mode. A nonlinear system is defined by the state and output equations:

$$\dot{x}(t) = f(x(t), u(t))$$
 Eq. (27)

$$y(k) = g(x(t), u(t))$$
 Eq. (28)

Let (x_0, u_0) be the states and control inputs at the equilibrium point around which the dynamic system is linearized:

$$\delta x(t) = x(t) - x_0$$
 Eq. (29)

$$\delta u(t) = u(t) - u_0$$
 Eq. (30)

$$\frac{\delta x(t)}{dx} = \dot{x} = f(x(t), u(t))$$
 Eq. (31)

FIGURE 6 Experimental validation for the <u>HCCI model</u> under steady-state condition (N = 800 RPM, T_{man} = 313-373 K, PR = 0-40). e_{avg} is the average error while σ_{err} is the standard deviation of error.

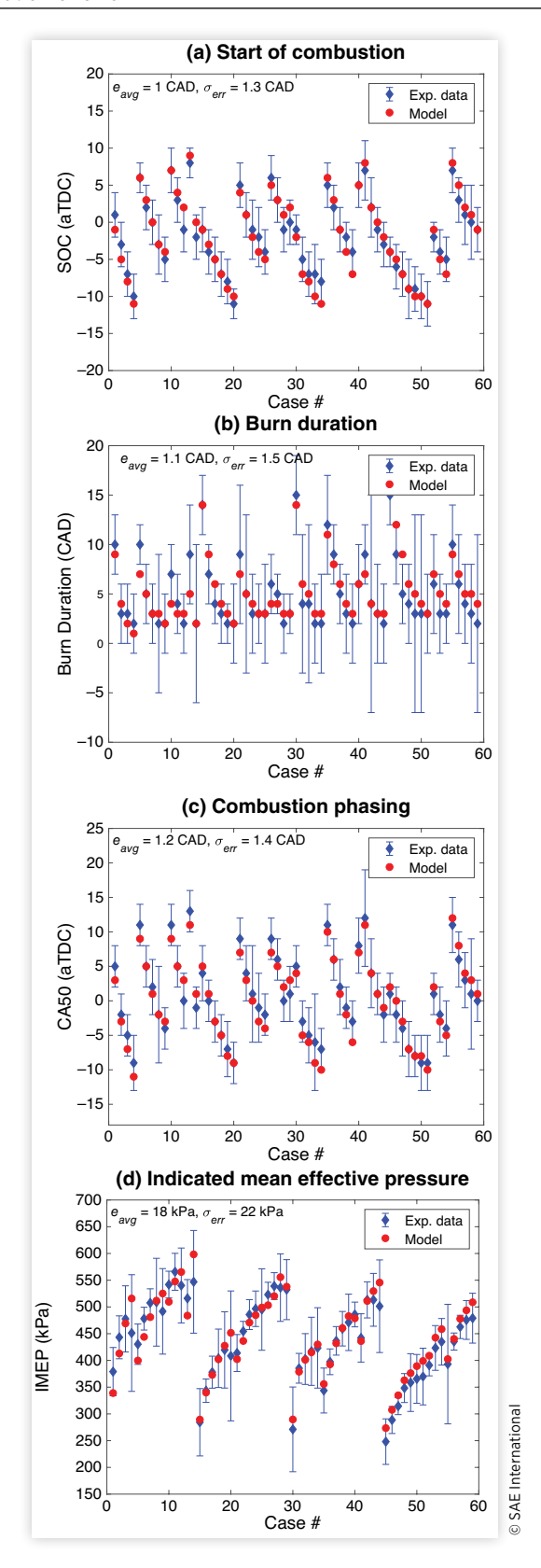


FIGURE 7 Experimental validation for the <u>PPCI model</u> under steady-state condition (N = 800 RPM, T_{man} = 313-373 K, PR = 0-40). e_{avg} is the average error while σ_{err} is the standard deviation of error.

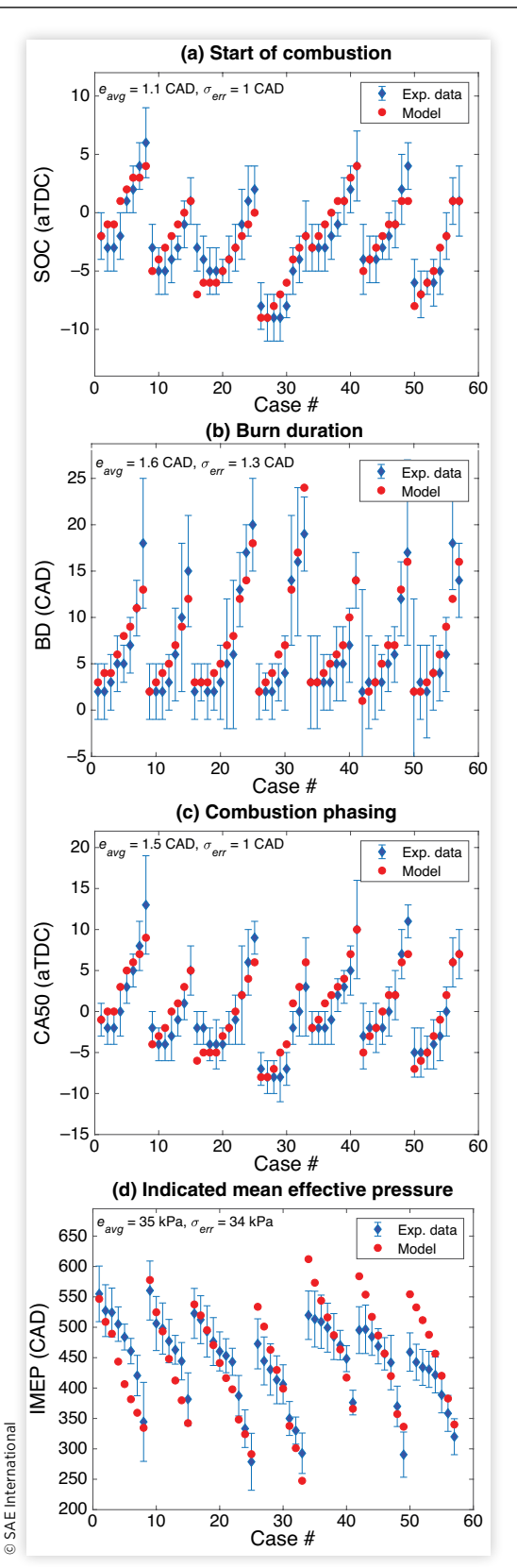


FIGURE 8 Experimental validation for the <u>RCCI model</u> under steady-state condition (N = 1000 RPM, T_{man} = 313 K, PR = 0-40, SOI = 20-60 CAD bTDC). e_{avg} is the average error while σ_{err} is the standard deviation of error.

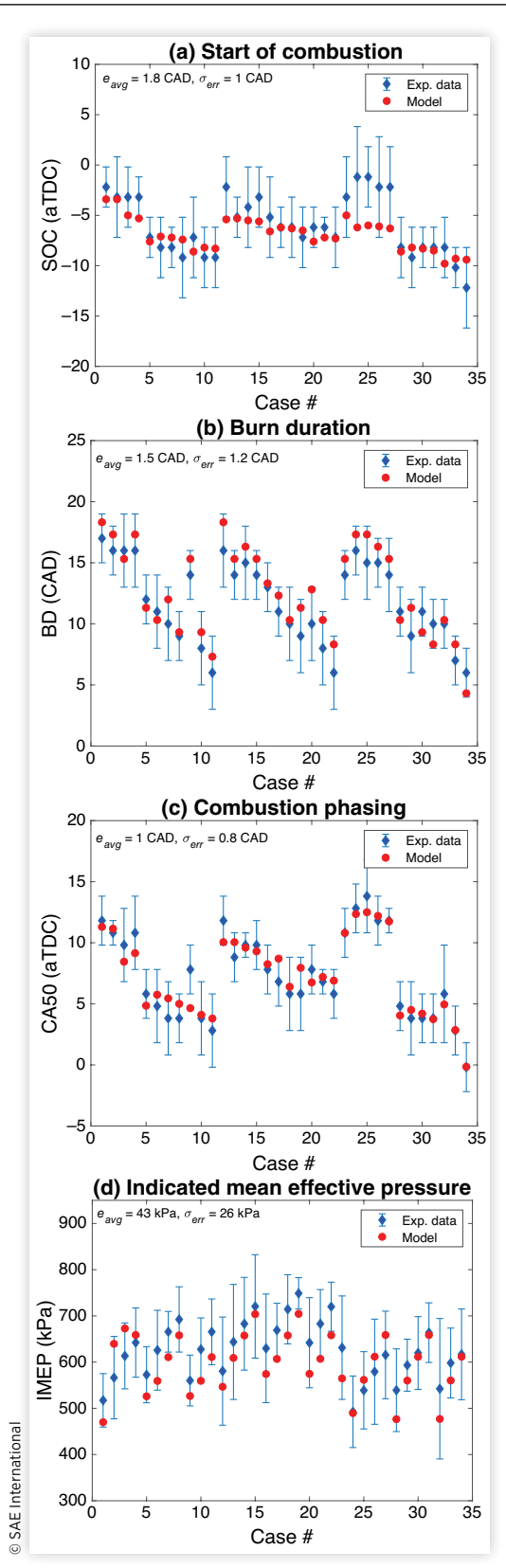
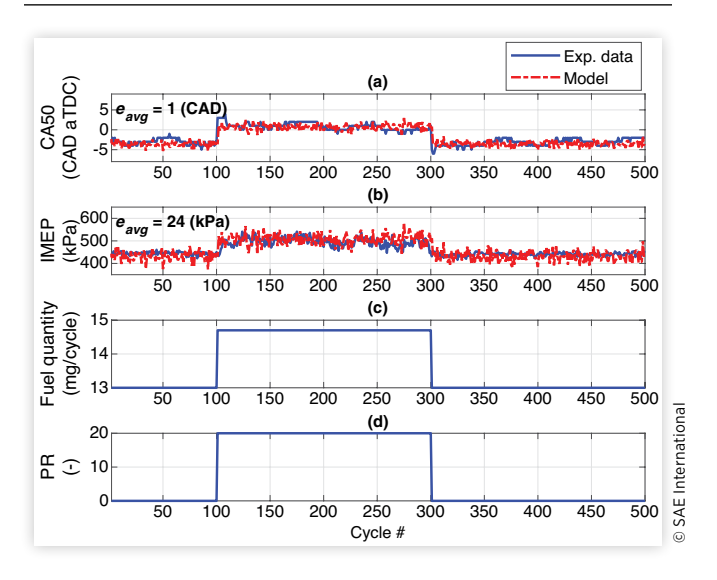


FIGURE 9 Experimental validation for the <u>HCCI COM model</u> under transient operation (N = 800 RPM, $T_{man} = 353$ K, SOI = 450 CAD bTDC).



By computing the Jacobian matrix of Eq. (27) w.r.t the states, we obtained

$$\begin{bmatrix} \delta \dot{x}_{1}(t) \\ \vdots \\ \delta \dot{x}_{4}(t) \end{bmatrix} = \begin{bmatrix} \frac{\delta f_{1}(t)}{x_{1}} & \dots & \frac{\delta f_{1}(t)}{x_{4}} \\ \vdots & \ddots & \vdots \\ \frac{\delta f_{4}(t)}{x_{1}} & \dots & \frac{\delta f_{4}(t)}{x_{4}} \end{bmatrix}_{(x_{0},u_{0})} \begin{bmatrix} \delta x_{1}(t) \\ \vdots \\ \delta x_{4}(t) \end{bmatrix}$$

$$+ \begin{bmatrix} \frac{\delta f_{1}(t)}{u_{1}} & \dots & \frac{\delta f_{1}(t)}{u_{4}} \\ \vdots & \ddots & \vdots \\ \frac{\delta f_{4}(t)}{u_{4}} & \dots & \frac{\delta f_{4}(t)}{u_{4}} \end{bmatrix} \begin{bmatrix} \delta u_{1}(t) \\ \vdots \\ \delta u_{4}(t) \end{bmatrix} + \begin{bmatrix} f_{1}(x_{0},u_{0}) \\ \vdots \\ f_{4}(x_{0},u_{0}) \end{bmatrix}$$
Eq. (32)

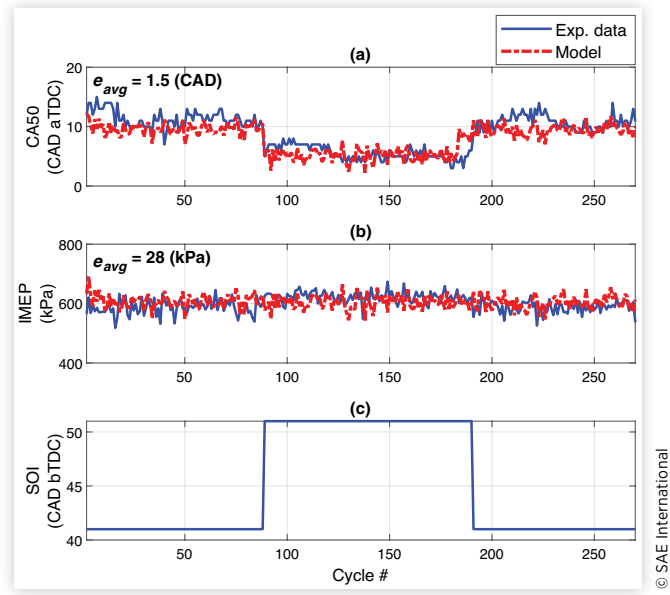
For the equilibrium point (x_0, u_0) ,

$$\begin{bmatrix} f_1(x_0, u_0) \\ \vdots \\ f_4(x_0, u_0) \end{bmatrix} = 0$$
 Eq. (33)

 δx is obtained by solving Equation 32 for δu and x(t) is computed. The linearized equations for the outputs are obtained in an analogous manner.

Based on the performance characterization, the nominal intake air temperatures are chosen to be 80°C, 40°C, and 60°C for HCCI, PPCI, and RCCI modes, respectively. The PR is used to control CA50 in HCCI and PPCI modes while SOI is used to control CA50 in RCCI mode. IMEP in each LTC mode is controlled by adjusting the FQ. In HCCI and PPCI modes, intake air temperature is modeled as a disturbance input while PR is modeled as a disturbance input in the RCCI mode.

FIGURE 10 Experimental validation for the <u>RCCI COM</u> model under transient operation due to step change in SOI (N = 1000 RPM, $T_{man} = 333 \text{ K}$, PR = 20, FQ = 23 mg/cycle).



$$CA50_{k+1} = f(CA50, T_{soc}, P_{soc}, IMEP, PR, FQ, T_m)_k$$
 Eq. (34)

$$IMEP_{k+1} = f(CA50, T_{soc}, P_{soc}, IMEP, PR, FQ, T_m)_k$$
 Eq. (35)

$$CA50_{k+1} = f(CA50, T_{soc}, P_{soc}, IMEP, SOI, FQ, PR)_{k}$$

Eq. (36)

$$IMEP_{k+1} = f(CA50, T_{soc}, P_{soc}, IMEP, SOI, FQ, PR)_k$$

Eq. (37)

The states of the MIMO COM of HCCI, PPCI, and RCCI are CA50, T_{soc} , P_{soc} , and IMEP. In addition, CA50 and IMEP are the outputs of the MIMO COM of HCCI, PPCI, and RCCI.

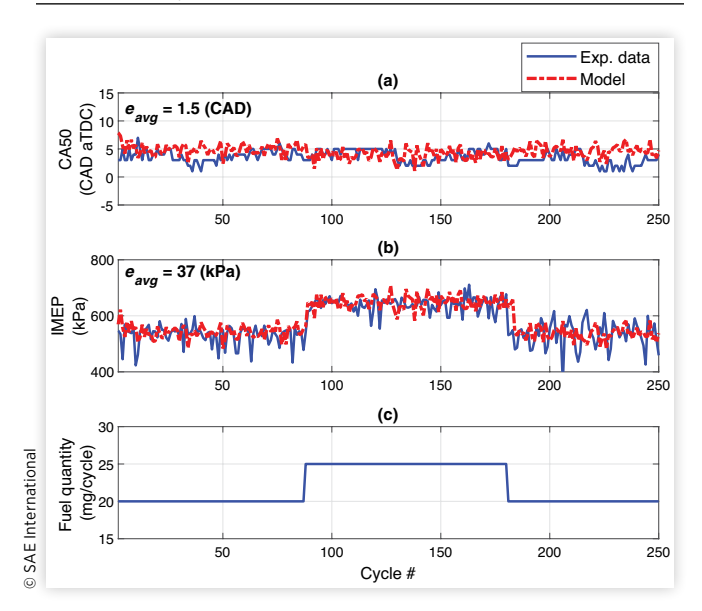
The linearization yields the following state space matrices for the HCCI model:

$$A = \begin{bmatrix} 0.2067 & -0.1761 & 0.0179 & -0.0586 \\ -0.2798 & 0.0194 & 0.0938 & -0.0638 \\ -3.2405 & -0.6555 & 1.0898 & -1.0923 \\ -0.9657 & 0.7802 & 0.0072 & 0.1506 \end{bmatrix} \text{Eq. (38)}$$

$$B = \begin{bmatrix} 0.3558 & -1.0438 \\ 0.1957 & -1.2902 \\ 1.8241 & 31.5290 \\ 0.9085 & 30.1506 \end{bmatrix}$$
Eq. (39)

$$B_{\nu} = \begin{bmatrix} 0.3915 \\ 1.8087 \\ 0.0380 \\ -2.4140 \end{bmatrix}$$
 Eq. (40)

FIGURE 11 Experimental validation for the <u>RCCI COM</u> model under transient operation due to step change in FQ (N = 1000 RPM, $T_{man} = 333 \text{ K}$, SOI = 50 CAD (bTDC), PR = 20).



$$C = \begin{bmatrix} 1 & 0 & 0 & 0 \\ 0 & 0 & 0 & 1 \end{bmatrix}$$
 Eq. (41)

$$D = \begin{bmatrix} 0 & 0 \\ 0 & 0 \end{bmatrix}$$
 Eq. (42)

The state-space matrices for the PPCI model are as follows:

$$A = \begin{bmatrix} 0.4602 & -0.0516 & -0.0009 & -0.0102 \\ 0.9645 & 0.7823 & 0.0147 & 0.0806 \\ 0.1369 & 0.5456 & 0.8911 & 0.0987 \\ -1.2572 & 0.7840 & 0.0092 & 0.4497 \end{bmatrix}$$
Eq. (43)

$$B = \begin{vmatrix} 0.1810 & -0.4005 \\ -0.2562 & -1.8488 \\ -0.1300 & -1.6146 \\ 0.0705 & 18.0950 \end{vmatrix}$$
 Eq. (44)

$$B_{\nu} = \begin{bmatrix} 0.0027 \\ 0.5479 \\ -0.8427 \\ -1.3600 \end{bmatrix}$$
 Eq. (45)

$$C = \begin{bmatrix} 1 & 0 & 0 & 0 \\ 0 & 0 & 0 & 1 \end{bmatrix}$$
 Eq. (46)

$$D = \begin{bmatrix} 0 & 0 \\ 0 & 0 \end{bmatrix}$$
 Eq. (47)

The following are the state-space matrices after linearizing the RCCI model:

$$A = \begin{bmatrix} 0.0393 & -0.0140 & 0.0052 & 0.0081 \\ -0.2741 & 0.0974 & -0.0361 & -0.0566 \\ -0.3965 & -0.1409 & -0.0523 & -0.0819 \\ 0.3743 & -0.1043 & 0.0493 & -0.0452 \end{bmatrix}$$
Eq. (48)

$$B = \begin{bmatrix} -0.4165 & -0.3176 \\ 0.4479 & 2.4402 \\ 4.2019 & 3.1550 \\ 2.1777 & 28.2946 \end{bmatrix}$$
Eq. (49)

$$C = \begin{bmatrix} 1 & 0 & 0 & 0 \\ 0 & 0 & 0 & 1 \end{bmatrix}$$
 Eq. (50)

$$D = \begin{bmatrix} 0 & 0 \\ 0 & 0 \end{bmatrix}$$
 Eq. (51)

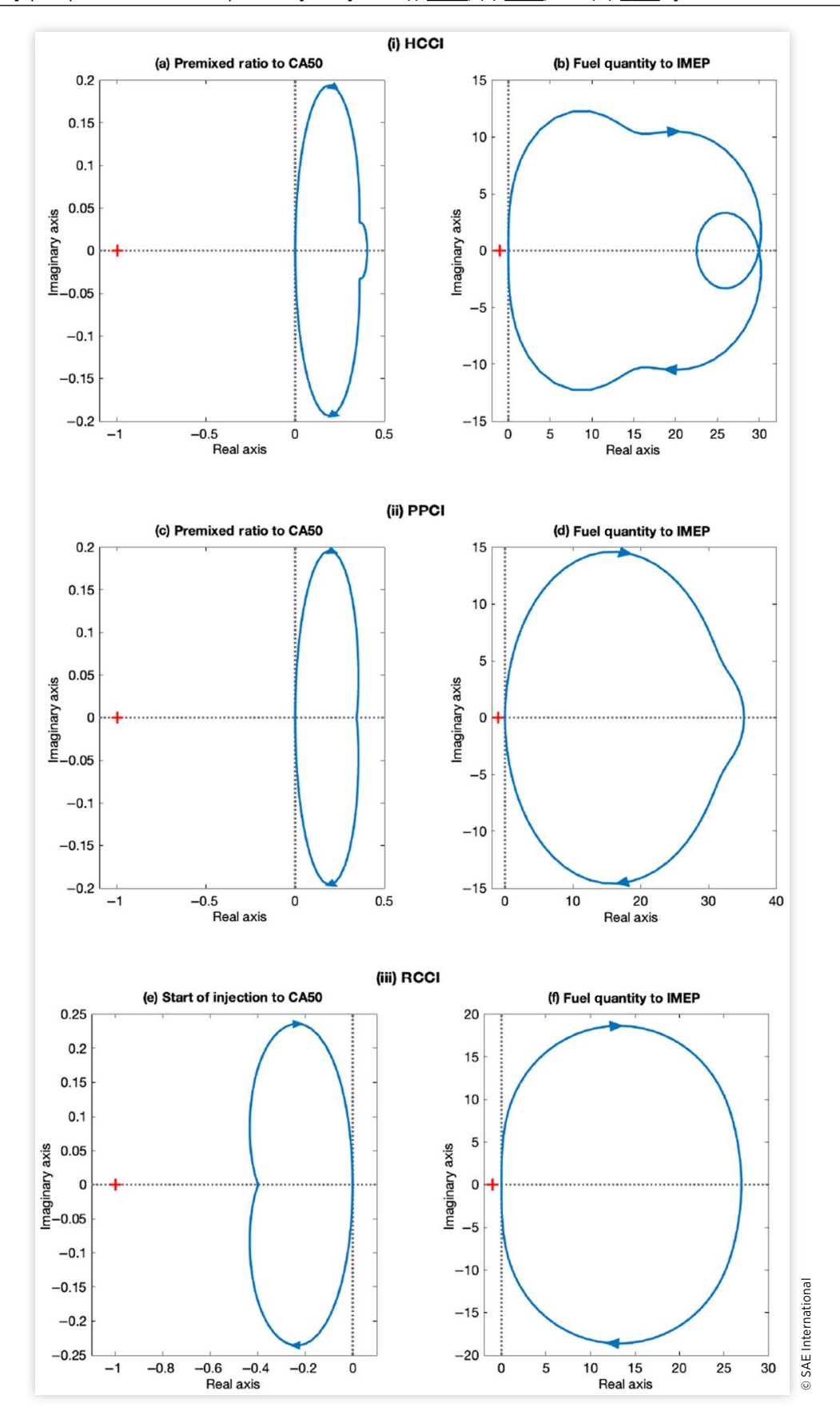
The linearized systems have been analyzed for open- and closed-loop stability. The discrete-time system is said to be asymptotically stable if the eigenvalues of the system lie within the unit circle [72]. The eigenvalues of HCCI, PPCI, and RCCI are presented in Table 3. The eigenvalues of the three LTC modes are within the unit circle; therefore, the systems are open-loop stable. Nyquist stability criteria is used to determine the closed-loop stability of the systems. CA50 is controlled by adjusting the PR of the dual fuels while IMEP is regulated by controlling the amount of injected FQ. Therefore, transfer functions are determined from inputs to outputs of the system, and the frequency response of a unity feedback system is plotted on the Nyquist diagram for each LTC mode. According to Nyquist stability criteria, if the contour encircles the entire right half-plane is mapped through the transfer functions of the system (G(s)) and unity feedback (H(s)), then the number of closed-loop poles (Z) of the unity feedback system in the right half-plane is equal to the number of clockwise revolutions (N) around the point (-1+0i) of the mapping minus the number of open-loop poles (P) that lie in the right half-plane, i.e., N = Z - P [72].

<u>Figures 12(a)</u> and <u>12(b)</u> show that the system is closed-loop stable because the open-loop poles of the HCCI system lie in the left half-plane and the point (-1 + 0i) lies outside the contour that maps the entire right half-plane. Therefore, the HCCI system is closed-loop stable. Based on Nyquist stability

TABLE 3 Eigenvalues of the linearized discrete-time open-loop system in the three LTC modes.

Modes	Eigenvalues
HCCI	0.92, -0.04, 0.08, 0.50
PPCI	0.30, 0.95, 0.61, 0.71
RCCI	0.18 + 0i, -0.0002 + 0i, -0.071 ± 0.043i

FIGURE 12 Nyquist plots for closed-loop stability analysis of (i) HCCI, (ii) PPCI, and (iii) RCCI systems.

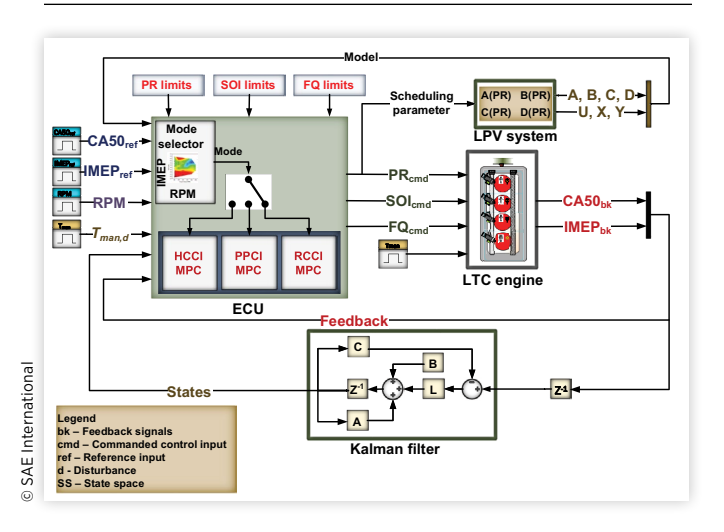


criteria, the contour mapped through the transfer functions of the system and unity feedback do not encircle the point (-1+0i) and the number of open-loop poles in the right halfplane (P)=0, as shown in Figures 12(c) and 12(d). This means that no closed-loop pole of PPCI mode exists in the right half-plane; thus, the closed-loop system is stable. Nyquist plots of RCCI show that the system is stable as the point (-1+0i) lies outside the contours of the transfer functions, as shown in Figures 12(e) and 12(f).

Controller Development

The LTC modes under study are operated using dual fuels, and changing the PR of two fuels affects the combustion process. Due to the highly nonlinear nature of the combustion process, a single MPC can only perform well in a limited region around the nominal operating conditions. Raut et al. developed multiple MIMO MPCs, each MPC capable of achieving the desired CA50 and IMEP for a range of PR. Therefore, PR is used as a scheduling variable to switch between the multiple MPCs to achieve the desired performance [21]. In this study, the limited operating regime of a single MPC is extended without any performance degradation by using the LPV models. The LPV models are capable of capturing the system dynamics which vary as a function of the time-varying scheduling parameter. The LPV system is represented as a linear state-space model with coefficients being the function of a scheduling parameter. In this study, the LPV models as a function of different values of PR are developed offline for each LTC mode. The LPV models update the internal predictive model at each control interval and are used within an adaptive MPC to achieve the nonlinear control. The schematic of the designed LPV-MPC system is shown in Figure 13. By using LPV models, the development of multiple MPCs can be avoided to cover a wide range of engine

FIGURE 13 Schematic of the designed adaptive MPC combustion controller with LPV systems to control CA50 and IMEP.



operations. Hence, the dynamic COM for the LTC modes can be represented in a discrete-time state-space model as a function of PR (scheduling parameter), as shown in <u>Equations</u> 52 and 53.

$$X_{k+1} = A(p)X_k + B(p)U_k$$
 Eq. (52)

$$Y_k = C(p)X_k + D(p)U_k$$
 Eq. (53)

X, U, and Y represent the states, control inputs, and outputs of the system. The states and outputs for the LTC modes are

$$X = \begin{bmatrix} CA50 & T_{soc} & P_{soc} & IMEP \end{bmatrix}^T$$
 Eq. (54)

$$Y = \begin{bmatrix} CA50 & IMEP \end{bmatrix}^T$$
 Eq. (55)

Control inputs for HCCI and PPCI modes are represented in <u>Equation 56</u>; while for RCCI, control inputs are presented in <u>Equation 57</u>. PR in <u>Equation 58</u> is used as a scheduling variable for the LTC modes.

$$U_{HCCL,PPCI} = \begin{bmatrix} PR & FQ \end{bmatrix}^T$$
 Eq. (56)

$$U_{RCCI} = \begin{bmatrix} SOI & FQ \end{bmatrix}^T$$
 Eq. (57)

$$p_{k} = \lceil PR \rceil$$
 Eq. (58)

The problem statement includes an optimal control objective of a MIMO system with a set of constraints on inputs and outputs for each combustion mode. Based on the targeted performance index, MIMO adaptive MPCs are developed for each combustion mode. An MPC is a real-time model-based optimization framework which provides flexibility in handling constraints on inputs, outputs, and states. An MPC requires information about the reference input over the prediction horizon, as shown in Equation 59. For all LTC modes, the prediction and control horizons are chosen to be five and three engine cycles, respectively. The output of the MPC over the prediction horizon presented in Equation 59 can be simplified in terms of states and control inputs as shown in Equation 60.

$$Y_{k} = [y(k+1|k \ y(k+2|k \ y(k+3|k \ y(k+4|k \ y(k+5|k)]^{T})]$$
Eq. (59)

$$Y_k = FX_k + \phi U_k$$
 Eq. (60)

where the matrices F and ϕ are computed by using <u>Equations</u> 61 and 62.

$$F = \begin{bmatrix} CA \\ CA^2 \\ CA^3 \\ CA^4 \\ CA^5 \end{bmatrix}$$
 Eq. (61)

$$\phi = \begin{bmatrix} CB & 0 & 0 & 0 & 0 \\ CAB & CB & 0 & 0 & 0 \\ CA^{2}B & CAB & CB & 0 & 0 \\ CA^{3}B & CA^{2}B & CAB & CB & 0 \\ CA^{4}B & CA^{3}B & CA^{2}B & CAB & CB \end{bmatrix}$$
Eq. (62)

The objective function is as follows:

$$J = \sum_{i=1}^{N} \left[\left(\Psi - Y_i \right)^T Q \left(\Psi - Y_i \right) + U^T R U \right] \qquad \text{Eq. (63)}$$

where *Q* and *R* are the weight matrices for reference tracking and control variables, respectively. The optimal solution for the control signal is given by

$$U = \left(\phi^T Q \Phi + R\right)^{-1} \phi^T Q \left(\Psi - FX(k)\right)$$
 Eq. (64)

The term $(\phi^T Q \Phi + R)^{-1} \phi^T Q \Psi$ in Equation 64 refers to the set point change. The term $(-\phi^T Q \Phi + R)^{-1} \phi^T Q F X$ in Equation 64 corresponds to the state feedback control. Quadratic programming is used to evaluate the cost function for optimal control signal in the presence of constraints. The objective function with active constraints is given by

$$J = \frac{1}{2}U^T E U + U^T H$$
 Eq. (65)

subject to constraints

$$A_{cons}U = B_{cons}$$
 Eq. (66)

where

$$E = \phi^T Q \phi + R; \quad H = \phi^T Q (\Psi - FX_k)$$
 Eq. (67)

The constraints on the manipulated variables for each LTC mode are applied. A_{cons} and B_{cons} matrices are given in Equation 68.

$$A_{cons} = \begin{bmatrix} I_{10\times10} \\ I_{10\times10} \end{bmatrix}; \quad B_{cons} = \begin{bmatrix} U_{max} - u(k_i - 1) \\ U_{min} + u(k_i - 1) \end{bmatrix} \text{ Eq. (68)}$$

MPC requires information about the state variables $(X(k_i))$ at the time (k_i) . It is expensive to use the sensors to measure all the states of the LTC engine. Thus, the state variables are estimated via an observer. To this end, a Kalman filter is used to estimate the unmeasured state variables like T_{soc} and P_{soc} for each mode. The developed adaptive MPCs with LPV systems are simulated in Matlab/Simulink.

Results and Discussion

The controller developed for HCCI mode is tested by providing step changes in IMEP and CA50. Measurement noise is added to both outputs in order to account for the measurement noise in real engine setup. The controller response is tested for a step of change of 8 CAD in CA50 and 100 kPa in IMEP. The controller response including the plant outputs and the manipulated variables is shown in Figure 14. It takes one engine cycle to attain the targeted CA50 for a step change in CA50. However, CA50 reaches the steady state in three engine cycles corresponding to the step change in the IMEP. The IMEP reaches its targeted value in one engine cycle corresponding to a step change of 100 kPa. The average errors in CA50 and IMEP with added measurement noises are 0.5 CAD and 7.6 kPa, respectively. In addition, the controller outputs remain within the set constraints of the actuators. For instance, when there is a step change in IMEP at Engine cycle #72, PR reaches its maximum value of 50 to maintain CA50 to its optimum value. One of the important performance characteristics of the controller is its disturbance rejection property. Thus, the designed controller is tested in the presence of disturbance input. Intake air temperature is modeled as disturbance input to the plant. A ramp signal for the change in intake air temperature is provided. The controller performance in the presence of disturbance is shown in Figure 15. The controller shows good disturbance rejection performance. It takes only one cycle for CA50 and IMEP to regain steadystate performance. In addition, there is no significant impact on the average errors of CA50 and IMEP. The controller performs well in tracking the step changes in CA50 and IMEP in the presence of disturbance input while meeting the set constraints.

FIGURE 14 Simulation results of MIMO adaptive MPC for step changes in IMEP and CA50 (HCCI mode). Operating conditions: N = 800 RPM, $T_{man} = 353$ K, $P_{man} = 96$ kPa.

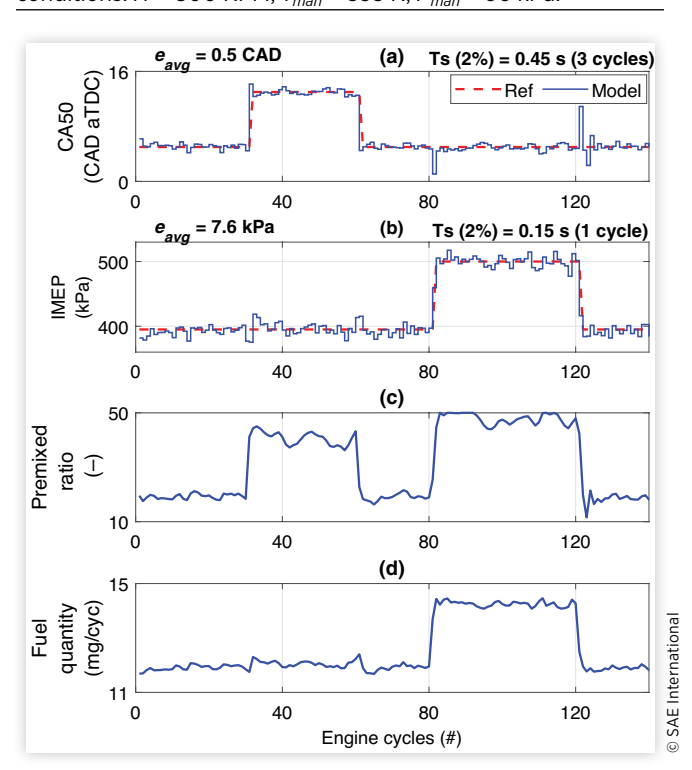
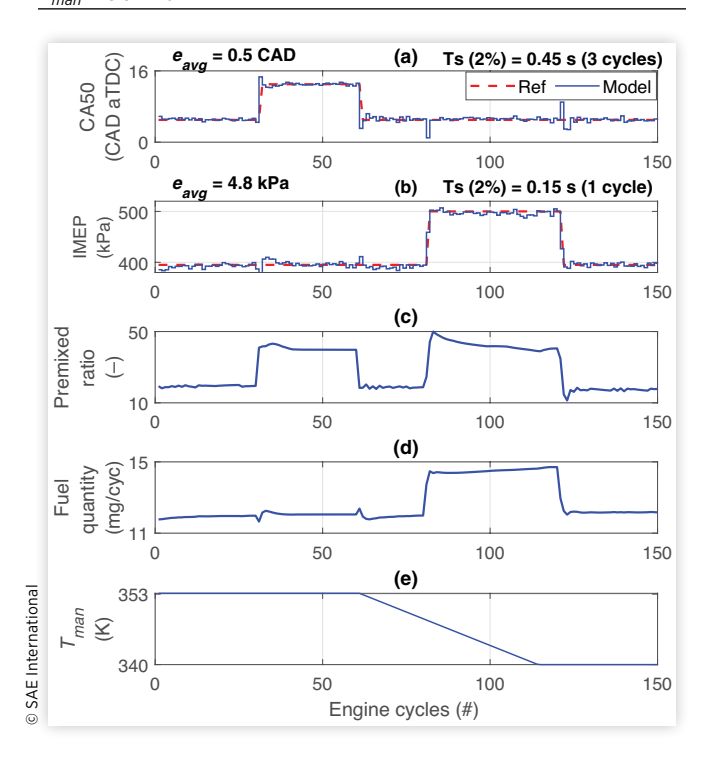


FIGURE 15 Disturbance rejection of MIMO adaptive MPC by varying T_{man} (HCCI mode). Operating conditions: N = 800 RPM, $P_{man} = 96$ kPa.



The performance of the MPC for PPCI mode is validated against the step changes in both CA50 and IMEP. CA50 and IMEP both reach the targeted value in one engine cycle against a step change in CA50. However, it takes 4 engine cycles to attain the targeted value of CA50 when there is a step change of 120 kPa in the required IMEP. IMEP takes one engine cycle to gain the steady state for a step change. The controller performance for reference tracking of CA50 and IMEP is shown in <u>Figure 16</u>. The average errors in tracking CA50 and IMEP are 0.2 CAD and 4.7 kPa, respectively. The controller performance is also tested in the presence of measured disturbance. The disturbance rejection performance of the controller is shown in Figure 17. A ramp change in the intake air temperature and a step change in IMEP are provided simultaneously. The controller is able to reject the disturbance in one engine cycle while it is able to track the targeted CA50 and IMEP.

For RCCI mode, the MPC is tested for two different cases. In the first case, the MPC is tested for the fuel with a fixed PR of 20. The controller performance is validated in the presence of two step changes in IMEP at different time steps while tracking the combustion phasing (CA50) to its optimum value. The IMEP reaches the target in one engine cycle while CA50 takes two engine cycles to attain the steady-state value. The controller response and plant outputs are shown in Figure 18. The average errors in tracking CA50 and IMEP are 0.2 CAD and 5.2 kPa, respectively. In the second case, the MPC for RCCI is tested for different PRs ranging from 5 to 45. For a step change of 5 in PR, CA50 takes one engine cycle to reach the optimum value while it takes two engine cycles for a step

change of 10 in PR. However, the IMEP regains the reference tracking in one engine cycle for both the step changes of 5 and 10 in PR. In addition, a step change of 200 kPa in IMEP is provided to test the controller performance for a range of PR. The controller is capable of tracking CA50 and IMEP without any performance degradation as shown in Figure 19.

Summary and Conclusions

This article presents model-based control development of three common LTC modes using dual fuels. The engine controller selects the best combustion regime based on the engine BSFC performance map. An independent combustion controller is developed for each mode which uses LPV models to capture the system dynamics for achieving the nonlinear LTC engine control. Major findings from this work for the tested conditions are

- Discrete-time COMs and LPV systems are developed as a function of dual-fuel PR for each LTC mode. The steady-state and transient validations show that the developed COMs are capable of predicting CA50 and IMEP on a cycle-to-cycle basis with average errors of less than 2 CAD and 37 kPa, respectively, for each LTC mode.
- For HCCI mode, the developed adaptive MPC uses PR and FQ to control CA50 and IMEP. Moreover, a PR is also used as a scheduling variable for the LPV system. Results show that the adaptive MPC with LPV system is able to track CA50 and IMEP with average errors of 0.5 CAD and 7.6 kPa, respectively. The controller is also tested for disturbance rejection properties.
- For PPCI mode, CA50 is controlled by adjusting the PR while IMEP is controlled by adjusting the FQ. The adaptive MPC uses PR as a scheduling variable for the LPV models. The controller performs well in the presence of measured disturbance. The average errors in CA50 and IMEP tracking are 0.1 CAD and 1.7 kPa, respectively.
- For RCCI mode, the SOI is used to control CA50 while the FQ is used for IMEP control. The PR is used as a scheduling variable to develop the LPV models. The adaptive MPC is able to track CA50 and IMEP with average errors of 0.2 CAD and 5.2 kPa, respectively.
- The MPCs developed for each mode are capable of providing good performance in controlling combustion phasing for any PR of fuels ranging between 0 and 50. This is because the LPV models with the PR as the scheduling parameter improve the performance of the controller by capturing the system dynamics. A single MPC with an LPV plant model works well for a wide range of PR both with and without disturbance inputs.

Overall, developed MPCs show promising results for reference tracking of CA50 and IMEP for the dual-fuel application in the LTC modes. Future work includes the real-time

FIGURE 16 Simulation results of MIMO adaptive MPC for step changes in IMEP and CA50 (<u>PPCI mode</u>). Operating conditions: N = 800 RPM, $T_{man} = 313$ K, $P_{man} = 96$ kPa.

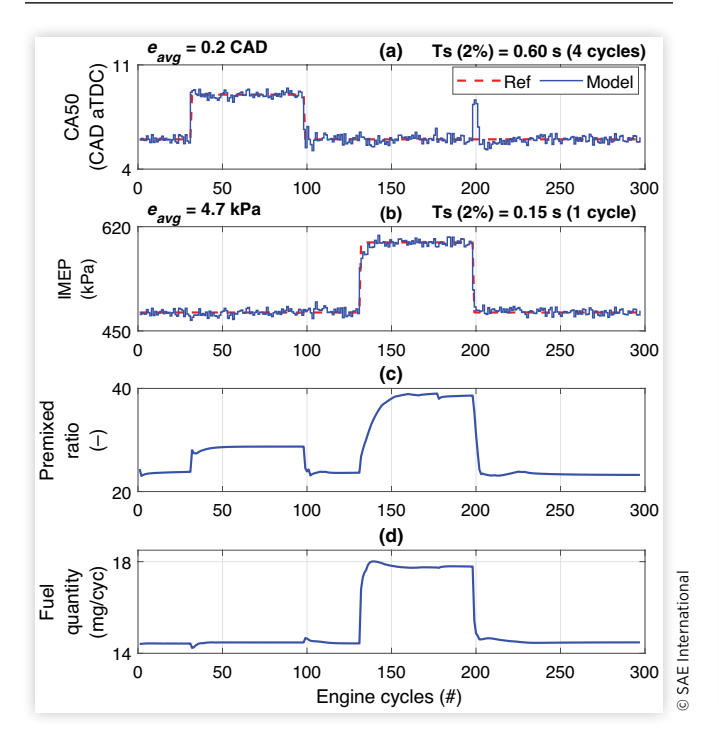


FIGURE 18 Simulation results of MIMO MPC for step changes in IMEP and CA50 (RCCI mode). Operating conditions: PR = 20, N = 1000 RPM, $T_{man} = 333$ K, $P_{man} = 96$ kPa.

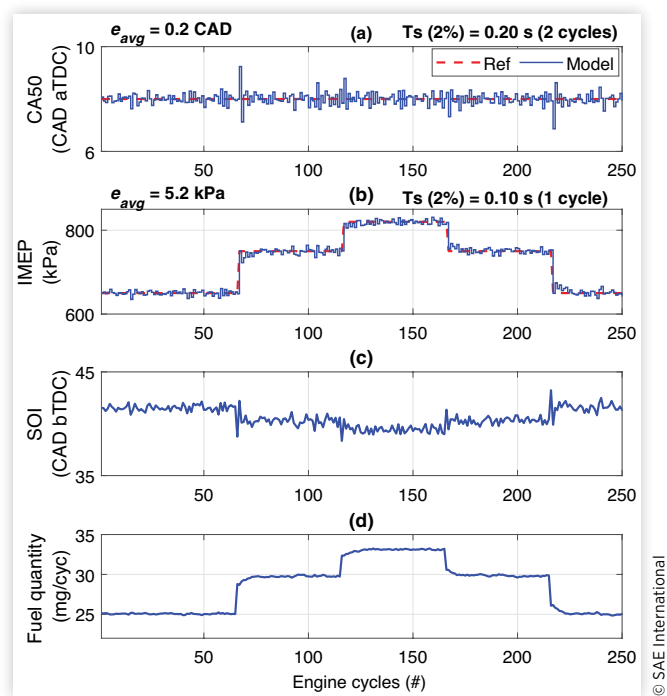


FIGURE 17 <u>Disturbance rejection</u> of MIMO adaptive MPC by varying T_{man} (<u>PPCI mode</u>). Operating conditions: N = 800 RPM, $P_{man} = 96$ kPa.

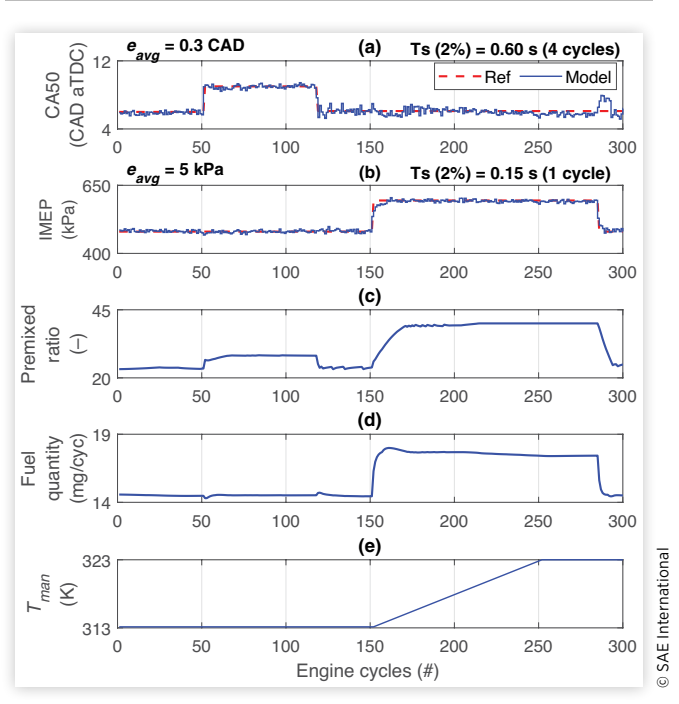
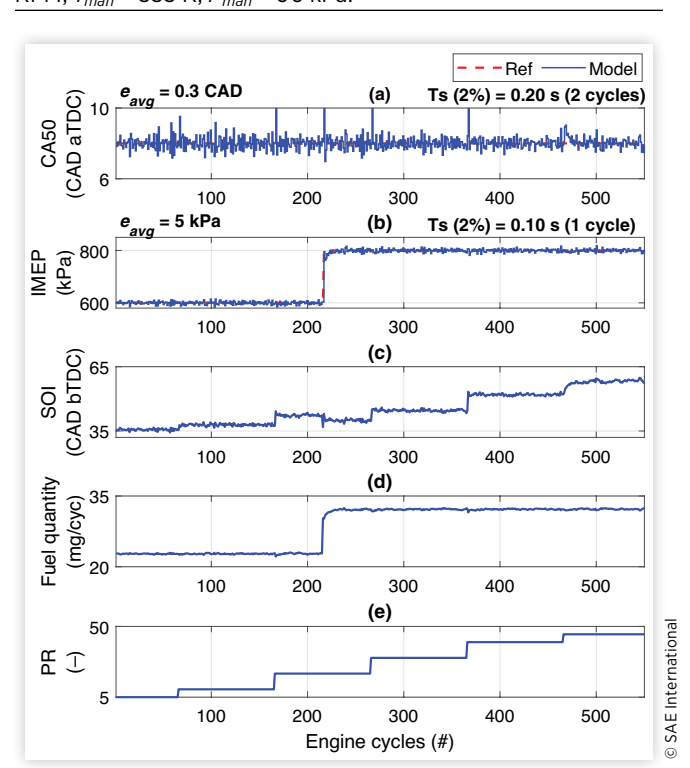


FIGURE 19 Simulation results of MIMO MPC for step changes in PR (RCCI mode). Operating conditions: N = 1000 RPM, $T_{man} = 333$ K, $P_{man} = 96$ kPa.



testing of these controllers on an actual LTC engine setup and also investigating the coupling LTC engine dynamics for mode-switching operation and design of mode-switching LTC controllers.

Acknowledgment

This work is supported by the Department of Energy-Hyundai (Grant# DE-EE0008478) and the U.S. National Science Foundation (Grant# 1762520). The authors would like to acknowledge the contributions of Dr. Seyfi Polat, Kaushik Kannan, and Akshat Raut.

Contact Information

Sadaf Batool

batool@mtu.edu

Jeffrey D. Naber

jnaber@mtu.edu

Mahdi Shahbakhti

mahdi@ualberta.ca

Nomenclature

Abbreviations

AFR - Air-to-fuel ratio

aTDC - After top dead center

bTDC - Before top dead center

CAD - Crank angle degrees

CI - Compression ignition

CoC - Completeness of combustion

DI - Direct injection

HCCI - Homogeneous charge compression ignition

ICE - Internal combustion engine

LHV - Lower heating value of fuel

LPV - Linear parameter varying

LTC - Low-temperature combustion

LQG - Linear quadratic Gaussian

MIMO - Multi-input and multi-output

MKIM - Modified knock integral model

NOx - Nitrogen oxides

ON - Octane number

PFI - Port fuel injection

PM - Particulate matter

PID - Proportional integral derivative controller

PPCI - Partially premixed charge compression ignition

RCCI - Reactivity controlled compression ignition

SI - Spark ignition

Parameters

BSFC - Brake specific fuel consumption (g/kWh)

CA50 - Combustion phasing (CAD aTDC)

 C_p - Specific heat capacity at constant pressure (kJ/kg K)

 C_r - Compression ratio

 C_{ν} - Specific heat capacity at constant volume (kJ/kg K)

EGR - Exhaust gas recirculation (%)

FQ - Fuel quantity (mg/cycle)

IAT - Intake air temperature (K)

IMEP - Indicated mean effective pressure (kPa)

 k_c - Ratio of specific heat capacities

 m_{iso} - Mass of iso-octane (mg/cycle)

 m_{nhep} - mass of *n*-heptane (mg/cycle)

MPRR - Maximum pressure rise rate (MPa/CAD)

N - Engine speed (RPM)

NMEP - Net mean effective pressure (kPa)

P - Pressure (kPa)

 p_k - Scheduling parameter (—)

PR - Premixed ratio (—)

R - Gas constant (kJ/kg K)

SOC - Start of combustion (CAD aTDC)

SOI - Start of injection (CAD bTDC)

T - Temperature (K)

V - Volume (m₃)

 X_d - Mixture dilution factor (—)

 $X_{r\sigma}$ - Residual gas fraction (—)

 $\boldsymbol{\theta}_d$ - Burn duration (CAD)

 λ - Air-to-fuel equivalence ratio

 ρ - Density (kg/m³)

 ϕ - Equivalence ratio

 ϕ_{DI} - Equivalence ratio of fuel via DI

 ϕ_{PFI} - Equivalence ratio of fuel injected via PFI

Subscripts

a - Air

dis - Displacement

eoc - End of combustion

evc - Exhaust valve closing

evo - Exhaust valve opening

exh - Exhaust

ivc - Intake valve closing

ivo - Intake valve opening

iso - Iso-octane

nhep - *n*-heptane

ref - Reference

rg - Residual gas

soc - Start of combustion

st - Stoichiometric

t - Total

References

- U.S. Energy Information Administration Office of Energy Analysis, "Annual Energy Outlook 2020 with Projections to 2050," 2020.
- Lü, X.-C., Chen, W., and Huang, Z., "A Fundamental Study on the Control of the HCCI Combustion and Emissions by Fuel Design Concept Combined with Controllable EGR. Part 1. the Basic Characteristics of HCCI Combustion," *Fuel* 84, no. 9 (2005): 1074-1083.
- Gorzelic, P.H., "Modeling and Model-Based Control of Multimode Combustion Engines for Closed-Loop SI/HCCI Mode Transitions with Cam Switching Strategies," PhD thesis, University of Michigan, 2015.
- 4. Manente, V., Johansson, B., and Tunestal, P., "Characterization of Partially Premixed Combustion with Ethanol: EGR Sweeps, Low and Maximum Loads," *ASME J. Eng. Gas Turbines Power* 132, no. 8 (2010): 082802.
- Yin, L., Ingesson, G., Shamun, S., and Tunestal, P., "Sensitivity Analysis of Partially Premixed Combustion (PPC) for Control Purposes," SAE Technical Paper 2015-01-0884 (2015), https://doi.org/10.4271/2015-01-0884.
- Arora, J., "Design of Real-Time Combustion Feedback System and Experimental Study of an RCCI Engine for Control," Master's thesis, Michigan Technological University, 2016.
- Thring, R., "Homogeneous-Charge Compression-Ignition (HCCI) Engines," SAE Technical Paper <u>892068</u> (1989), https://doi.org/10.4271/892068.
- 8. Martinez-Frias, J., Aceves, S., Flowers, D., Smith, J. et al., "HCCI Engine Control by Thermal Management," SAE Technical Paper 2000-01-2869 (2000), https://doi.org/10.4271/2000-01-2869.
- 9. Haraldsson, G., Tunestål, P., Johansson, B., and Hyvönen, J., "HCCI Closed-Loop Combustion Control Using Fast Thermal Management," SAE Technical Paper 2004-01-0943 (2004), https://doi.org/10.4271/2004-01-0943.
- Shaver, G.M., Roelle, M., and Gerdes, J.C., "Modeling Cycleto-Cycle Coupling in HCCI Engines Utilizing Variable Valve Actuation," *IFAC Proceedings* 37, no. 22 (2004): 227-232.
- 11. Ravi, N., "Modeling and Control of Exhaust Recompression HCCI Using Variable Valve Actuation and Fuel Injection," PhD thesis, Stanford University, 2010.
- 12. Haraldsson, G., Tunestål, P., Johansson, B., and Hyvönen, J., "HCCI Combustion Phasing in a Multi Cylinder Engine

- Using Variable Compression Ratio," SAE Technical Paper 2002-01-2858 (2002), https://doi.org/10.4271/2002-01-2858.
- 13. Hyvönen, J., Haraldsson, G., and Johansson, B., "Operating Range in a Multi Cylinder HCCI Engine Using Variable Compression Ratio," SAE Technical Paper 2003-01-1829 (2003), https://doi.org/10.4271/2003-01-1829.
- Yao, C., Hu, Y., Zhou, T., Yang, F. et al., "Combustion Stability Control of Dieseline PPCI Based on In-Cylinder Pressure Signals," *IFAC-PapersOnLine* 49, no. 11 (2016): 333-339.
- Yin, L., Turesson, G., Tunestål, P., and Johansson, R., "Model Predictive Control of an Advanced Multiple Cylinder Engine with Partially Premixed Combustion Concept," *IEEE/ASME Transactions on Mechatronics* 25, no. 2 (2020): 804-814.
- 16. Wissink, M. and Reitz, R., "Direct Dual Fuel Stratification, a Path to Combine the Benefits of RCCI and PPC," *SAE Int. J. Engines* 8, no. 2 (2015): 878-889, https://doi.org/10.4271/2015-01-0856.
- 17. Ma, J., Lü, X., Ji, L., and Huang, Z., "An Experimental Study of HCCI-DI Combustion and Emissions in a Diesel Engine with Dual Fuel," *Int. J. Therm. Sci.* 47, no. 9 (2008): 1235-1242.
- Shahbakhti, M. and Koch, C.R., "Physics Based Control Oriented Model for HCCI Combustion Timing," ASME J. Dyn. Syst., Meas., Control 132, no. 2 (2010): 021010.
- Ravi, N., Liao, H., Jungkunz, A.F., Widd, A. et al., "Model Predictive Control of HCCI Using Variable Valve Actuation and Fuel Injection," Cont. Eng. Pract. 20 (2012): 421-430.
- 20. Benajes, J., Tormos, B., Garcia, A., and Monsalve-Serrano, J., "Impact of Spark Assistance and Multiple Injections on Gasoline PPC Light Load," *SAE Int. J. Engines* 7, no. 4 (2014): 1875-1887, https://doi.org/10.4271/2014-01-2669.
- 21. Raut, A., Bidarvatan, M., Borhan, H., and Shahbakhti, M., "Model Predictive Control of an RCCI Engine," in 2018 Annual American Control Conference (ACC), Milwaukee, WI, 1604-1609, 2018.
- 22. Ibron, C., Jangi, M., Lonn, S., Matamis, A. et al., "Effect of Injection Timing on the Ignition and Mode of Combustion in a HD PPC Engine Running Low Load," SAE Technical Paper 2019-01-0211 (2019), https://doi.org/10.4271/2019-01-0211.
- Batool, S., Naber, J.D., and Shahbakhti, M., "Multi-Mode Low Temperature Combustion (LTC) and Mode Switching Control," in: Agarwal, A.K., Martínez, A.G., Kalwar, A., and Valera, H. (eds), Advanced Combustion for Sustainable Transport. Energy, Environment, and Sustainability (Singapore: Springer, 2022).
- Shahbakhti, M., Lupul, R., and Koch, C.R., "Sensitivity Analysis & Modeling of HCCI Auto-Ignition Timing," *IFAC Proceedings* 40, no. 10 (2007): 303-310.
- Dempsey, A.B., Walker, N.R., Gingrich, E., and Reitz, R.D., "Comparison of Low Temperature Combustion Strategies for Advanced Compression Ignition Engines with a Focus on Controllability," Comb. Sci. Technol. 186, no. 2 (2014): 210-241.
- 26. Divekar, P., Asad, U., Han, X., Chen, X. et al., "Study of Cylinder Charge Control for Enabling Low Temperature

- Combustion in Diesel Engines," J. Eng. Gas Turbines Power 136, no. 9 (2014): 091503.
- 27. Noehre, C., Andersson, M., Johansson, B., and Hultqvist, A., "Characterization of Partially Premixed Combustion," SAE Technical Paper 2006-01-3412 (2006), https://doi.org/10.4271/2006-01-3412.
- 28. Indrajuana, A., Bekdemir, C., Luo, X., and Willems, F., "Robust Multivariable Feedback Control of Natural Gas-Diesel RCCI Combustion," *IFAC-PapersOnLine* 49, no. 11 (2016): 217-222.
- Splitter, D., Wissink, M., DelVescovo, D., and Reitz, R., "RCCI Engine Operation Towards 60% Thermal Efficiency," SAE Technical Paper 2013-01-0279 (2013), https://doi. org/10.4271/2013-01-0279.
- Splitter, D., Hanson, R., Kokjohn, S., Wissink, M. et al., "Injection Effects in Low Load RCCI Dual-Fuel Combustion," SAE Technical Paper 2011-24-0047 (2011), https://doi.org/10.4271/2011-24-0047.
- 31. Wu, Y., Hanson, R., and Reitz, R.D., "Investigation of Combustion Phasing Control Strategy during Reactivity Controlled Compression Ignition (RCCI) Multicylinder Engine Load Transitions," *ASME J. Eng. Gas Turbines Power* 136, no. 9 (2014): 091511.
- 32. Fathi, O.J.M. and Shahbakhti, M., "Modeling and Controller Design Architecture for Cycle-by-Cycle Combustion Control of Homogeneous Charge Compression Ignition (HCCI) Engines—A Comprehensive Review," *Energy Conversion and Management* 139 (2017): 1-19.
- 33. Olsson, J., Tunestål, P., and Johansson, B., "Closed-Loop Control of an HCCI Engine," SAE Technical Paper 2001-01-1031 (2001), https://doi.org/10.4271/2001-01-1031.
- Strandh, P., Bengtsson, J., Johansson, R., Tunestål, P. et al., "Cycle-to-Cycle Control of a Dual-Fuel HCCI Engine," SAE Technical Paper 2004-01-0941 (2004), https://doi. org/10.4271/2004-01-0941.
- Bengtsson, J., Strandh, P., Johansson, R., Tunestål, P. et al., "Multi-Output Control of a Heavy Duty HCCI Engine Using Variable Valve Actuation and Model Predictive Control," SAE Technical Paper 2006-01-0873 (2006), https://doi. org/10.4271/2006-01-0873.
- Widd, A., Liao, H., Gerdes, J.C., Tunestål, P. et al., "Control of Exhaust Recompression HCCI Using Hybrid Model Predictive Control," in *Proceedings of the 2011 American Control Conference*, San Francisco, CA, 420-425, 2011.
- 37. Shaver, G.M., Gerdes, J.C., and Roelle, M.J., "Physics-Based Modeling and Control of Residual-Affected HCCI Engines," *ASME J. Dyn. Syst., Meas., Control* 131, no. 2 (2009): 021002.
- Kang, J. and Druzhinina, M., "HCCI Engine Control Strategy with External EGR," in *Proceedings of the 2010 American Control Conference*, Baltimore, MD, 3783-3790, 2010.
- Ebrahimi, K. and Koch, C., "Model Predictive Control for Combustion Timing and Load Control in HCCI Engines," SAE Technical Paper 2015-01-0822 (2015), https://doi. org/10.4271/2015-01-0822.
- 40. Bidarvatan, M., Kothari, D., and Shahbakhti, M., "Integrated Cycle-to-Cycle Control of Exhaust Gas Temperature, Load,

- and Combustion Phasing in an HCCI Engine," in 2015 American Control Conference (ACC), Chicago, IL, 7-12, 2015.
- 41. Ingesson, G., Yin, L., Johansson, R., and Tunestål, P., "A Double-Injection Control Strategy for Partially Premixed Combustion," *IFAC-PapersOnLine* 49, no. 11 (2016): 353-360.
- 42. Yang, T., Yin, L., Meng, X., Tian, H. et al., "Partially Premixed Combustion Optimization Using Double Injection Strategy in Transient Operation," *Appl. Therm. Eng.* 169 (2020): 114963.
- 43. Kondipati, N.T., "Experimental Study, Modelling and Controller Design for an RCCI Engine," Master's thesis, Michigan Technological University, 2016.
- 44. Sadabadi, K.K., "Modelling and Control of an RCCI Engine," Master's thesis, Michigan Technological University, 2015.
- Tandra, V. and Srivastava, N., "Optimal Peak Pressure and Exhaust Temperature Tracking Control for a Two-Zone HCCI Engine Model with Mean Burn Duration," SAE Technical Paper <u>2009-01-1130</u> (2009), https://doi.org/10.4271/2009-01-1130.
- 46. Asad, U., Zheng, M., Tjong, J., and Wang, M., "EC1-1 A Control Strategy Analysis for Clean and Efficient Combustion in Compression Ignition Engines," The Proceedings of the International Symposium on Diagnostics and Modeling of Combustion in Internal Combustion Engines 2012, no. 8 (2012): 251-256.
- 47. Asad, U. and Zheng, M., "Diesel Pressure Departure Ratio Algorithm for Combustion Feedback and Control," *Int. J. Engine Res.* 15, no. 1 (2014): 101-111.
- 48. Hellstrom, E., Larimore, J., Jade, S., Stefanopoulou, A.G. et al., "Reducing Cyclic Variability While Regulating Combustion Phasing in a Four-Cylinder HCCI Engine," *IEEE Trans. Control Syst. Technol.* 22, no. 3 (2014): 1190-1197.
- 49. Chiang, C., Stefanopoulou, A.G., and Jankovic, M., "Nonlinear Observer-Based Control of Load Transitions in Homogeneous Charge Compression Ignition Engines," *IEEE Trans. Control Syst. Technol.* 15, no. 3 (2007): 438-448.
- 50. Audet, A. and Koch, C.R., "Actuator Comparison for Closed Loop Control of HCCI Combustion Timing," SAE Technical Paper 2009-01-1135 (2009), https://doi.org/10.4271/2009-01-1135.
- Irdmousa, B.K., Rizvi, S.Z., Veini, J.M., Naber, J.D., and et al., "Data-Driven Modeling and Predictive Control of Combustion Phasing for RCCI Engines," in 2019 American Control Conference (ACC), Philadelphia, PA, 1617-1622, 2019.
- 52. Yin, L., Ingesson, G., Johansson, R., Tunestål, P. et al., "Model-Based Partially Premixed Combustion (PPC) Timing Control," *IFAC-PapersOnLine* 49, no. 11 (2016): 340-346.
- 53. Xia, L., de Jager, B., Donkers, T., and Willems, F., "Robust Constrained Optimization for RCCI Engines Using Nested Penalized Particle Swarm," *Control Eng. Pract.* 99 (2020): 104411.
- 54. Basina, L.N.A., Irdmousa, B.K., Velni, J.M., Borhan, H. et al., "Data-Driven Modeling and Predictive Control of Maximum Pressure Rise Rate in RCCI Engines," in *2020 IEEE*

- Conference on Control Technology and Application (CCTA), Montreal, QC, Canada, 94-99, 2020.
- Eichmeier, J., Reitz, R., and Rutland, C., "A Zero-Dimensional Phenomenological Model for RCCI Combustion Using Reaction Kinetics," SAE Int. J. Engines 7, no. 1 (2014): 106-119, https://doi.org/10.4271/2014-01-1074.
- Zhang, S., Zhu, G., and Sun, Z., "A Control-Oriented Charge Mixing and Two-Zone HCCI Combustion Model," *IEEE Trans. Veh. Technol.* 63, no. 3 (2014): 1079-1090.
- Shaver, G.M., Roelle, M., and Gerdes, J.C., "A Two-Input Control Model of HCCI Engines," in 2006 American Control Conference, Minneapolis, MN, 6, 2006.
- Shahbakhti, M. and Koch, C.R., "Control Oriented Modeling of Combustion Phasing for an HCCI Engine," in 2007 American Control Conference, New York, 3694-3699, 2007.
- 59. Ebrahimi, K., Koch, C., and Schramm, A., "A Control Oriented Model with Variable Valve Timing for HCCI Combustion Timing Control," SAE Technical Paper 2013-01-0588 (2013), https://doi.org/10.4271/2013-01-0588.
- Ebrahimi, K., Aliramezani, M., and Koch, C.R., "An HCCI Control Oriented Model that Includes Combustion Efficiency," *IFAC-PapersOnLine* 49, no. 11 (2016): 327-332.
- 61. Bidarvatan, M., Thakkar, V., Shahbakhti, M., Bahri, B. et al., "Grey-Box Modeling of HCCI Engines," *Appl. Therm. Eng.* 70, no. 1 (2014): 397-409.
- 62. Ravi, N., Roelle, M.J., Jungkunz, A.F. and Gerdes, J.C., "A Physically Based Two-State Model for Controlling Exhaust Recompression HCCI in Gasoline Engines," in *Proceedings of the ASME 2006 International Mechanical Engineering Congress and Exposition. Dynamic Systems and Control, Parts A and B*, Chicago, IL, 483-492, 2006.
- 63. Hall, C., Van Alstine, D., Kocher, L., Shaver, G. et al., "Combustion Timing Modeling and Control Framework for Biodiesel/Diesel Blends during Pre-Mixed Combustion," in Proceedings of the ASME 2012 5th Annual Dynamics Systems and Control Conference Joint with the JSME 2012 11th Motion and Vibration Conference, Fort Lauderdale, FL, 329-338, 2012.

- Tunestål, P. and Lewander, M., Model Predictive Control of Partially Premixed Combustion (London: Springer London, 2010), 171-181
- Batool, S., Naber, J.D., and Shahbakhti, M., "Data-Driven Modeling and Control of Cyclic Variability of an Engine Operating in Low Temperature Combustion Modes," *IFAC-PapersOnLine* 54, no. 20 (2021): 834-839.
- 66. Widd, A., Johansson, R., Borgqvist, P., Tunestal, P. et al., "Investigating Mode Switch from SI to HCCI Using Early Intake Valve Closing and Negative Valve Overlap," SAE Technical Paper 2011-01-1775 (2011), https://doi. org/10.4271/2011-01-1775.
- 67. Roelle, M.J., Shaver, G.M., and Gerdes, J.C., "Tackling the Transition: A Multi-Mode Combustion Model of SI and HCCI for Mode Transition Control," in ASME International Mechanical Engineering Conference and Exposition, Dynamic Systems and Control, Parts A and B, Arlington, VA, 329-336, 2004.
- 68. Nuesch, S.P., "Analysis and Control of Multimode Combustion Switching Sequence," PhD thesis, University of Michigan, 2015.
- 69. Kannan, K., "An Experimental Investigation of Low Temperature Combustion Regimes in a Light Duty Engine," Master's thesis, Michigan Technological University, 2016.
- Kokjohn, S., Reitz, R., and Musculus, M., "Investigation of Fuel Reactivity Stratification for Controlling PCI Heat-Release Rates Using High-Speed Chemiluminescence Imaging and Fuel Tracer Fluorescence," SAE Int. J. Engines 5, no. 2 (2012): 248-269, https://doi. org/10.4271/2012-01-0375.
- 71. Aquino, C., "Transient A/F Control Characteristics of the 5 Liter Central Fuel Injection Engine," SAE Technical Paper 810494 (1981), https://doi.org/10.4271/810494.
- 72. Gene, J.D.P., Franklin, F., and Emami-Naeini, A.F., *Feedback Control of Dynamic Systems*, 6th ed. (Upper Saddle River, NJ: Pearson, 2009.)

^{© 2023} SAE International. All rights reserved. No part of this publication may be reproduced, stored in a retrieval system, or transmitted, in any form or by any means, electronic, mechanical, photocopying, recording, or otherwise, without the prior written permission of SAE International.